Alignment and Sample Preparation of Conductive Polymer/Carbon Nanocone Adhesives for TEM

Petter Ingebrigtsen

Department of Physics

University of Oslo

Thesis is submitted in partial fulfilment

of the requirements for the degree of

Master of Science in Materials, Energy and Nanotechnology

June 1st 2012

Preface

This thesis is submitted to the Department of Physics, University of Oslo in partial fulfilment of the requirements for the degree of Master of Science in Materials, Energy and Nanotechnology.
The work was performed at Institute for Energy Technology (IFE), Department of Physics, and at the University of Oslo, Centre for Materials Science and Nanotechnology (SMN), during the period August 2010 to June 2012.

I would like to thank supervisors Anette E. Gunnæs for the all-helping guidance, Geir Helgesen for the project initiative and the theoretical foundation and Matti Knaapila for invaluable experimental support and motivation. I also thank Ole Bjørn Karlsen for technical support and Norbert Roos for assisting with cryo-ultramicrotomy sectioning.
A special thanks to my fellow students and co-workers, you made this so much more enjoyable.

Lastly, I would like to thank those close to me for support and encouragement, which were of great help.

Petter Ingebrigtsen
(University of Oslo, June 2012)

Abstract

The four primary forms of carbon known as graphite, diamond, fullerenes and carbon nanotubes have been previously been vigorously studied for a wide range of applications and functional materials. During the last decade a new form of carbon has been in the spotlight, which is the carbon nanocones. These carbon nanocones are virtually pure elemental carbon in the form of disks or cones in the range of 200 nm – 4000 nm in diameter.

Carbon nanocones are highly interesting as filler materials for conducting adhesives since they offer a cheap and inexhaustible supply of raw materials where the production is capable of easy upscaling to industrial production quantities, like carbon black. The advantage of using carbon nanocones as filler material in conducting adhesives instead of carbon black is the possibly increased conducting properties of the particles, and the bigger particles offers decreased overall resistance in the conductive adhesives due to fewer particle boundaries.

To explore conductive polymer/carbon nanocone adhesives further than previously by the use of transmission electron microscopy (TEM), composite samples were prepared in-plane and out-of-plane by dielectrophoretic alignment of particles induced by an external AC field. Selected sample preparation routes for TEM were tested to establish a working method of investigation to discover the inner structure of the composites, and were investigated in such a microscope. Cryo-Ultramicrotomy proved to be a successful method, although at a mediocre success rate and with limited area for investigation.

The results revealed that the particles have a point contact rather than a larger flat surface contact. In the prepared sample, the contacts seem to occur at the singular points of the particles, that is facets of disk edges and cones, and at the apex for the carbon cones. The point contact of the particles may explain why the electrical conductivity of aligned composites is easily disrupted by mechanical stress.

Wetting and filling of polymer/carbon were investigated by TEM and SEM, which revealed that electrowetting did not dominate the wetting properties.

Carbon nanocones were also investigated by HRTEM, and several interesting results were discovered.

The tip of the cones was discovered to have facets, with subsequent layers having the same layer faceting and adding up to a group of layers. Such groups of layers were shown to be divided by cavities in the tip which separates the groups with different faceting.

Facets at the circumference of the carbon nanocones were discovered, and these β-facets were also discovered to be highly non-uniform along the circumference of the cones. The layered structure of Carbon nanocones was discovered to have no domain-changes within a relatively large area, indicating single-domain layers throughout the particle.

Acronyms

AC – Alternating Current

ACAs – Anisotropic Conductive Adhesives

BF – Bright Field

BSE – Back-Scattered Electrons

BSU – Basic Structural Unit

CB – Carbon Black

CB&H - Kvaerner Carbon Black and Hydrogen Process

CNCs – Carbon Nanocone

CNTs – Carbon Nanotube

DC – Direct Current

DEP – Dielectrophoresis

DF – Dark Field

ECAs – Electrically Conductive Adhesives

EDS – Energy Dispersive X-Ray Spectroscopy

EM – Electron Microscopy/Microscope

FEG – Field Emission Gun

FIB – Focused Ion Beam

ICAs – Isotropic Conductive Adhesives

JEOL – Japanese Electron Optics Laboratory Co., Ltd

OM – Optical Microscopy/Microscope

SE – Secondary Electrons

SEM – Scanning Electron Microscopy/Microscope

SAD – Selected Area Diffraction

TEM – Transmission Electron Microscopy/Microscope

UM – Ultramicrotomy

Table of Contents

1. Introduction

In the modern world, increasing demands for advanced electronics have pushed the limits for traditional soldering methods. Energy hungry applications in modern electronics have led to reduced scales in all dimensions, and electronics packaging is an important field for managing the difficulties that arise. The traditional soldering methods are using environmentally unfriendly heavy metals, and the nature of soldering causes breakages at low dimensions due to mechanical stress [2]. The impact of such breakage may either degrade conductivity and performance, or it may break the connection permanently causing a system wide failure. Conventional solders cannot meet the requirements of the modern fine-pitch assembly due to their stencil printing resolution limit and bridging issues at low dimensions either [3].

Both the environmental concern aspect and the improvement of electronics require alternative methods, and to meet the demands, soldering is complimented by electrically conductive adhesives. While the field of research is relatively new there have been incredible advances the last few years, and some applications are already well established like the aforementioned lead-free soldering replacement for electronic packaging interconnects of flat electrodes and various other electronic applications [4]. The research is also well underway or at the starting phase in a broad band of applications like conductive inks [5], electromagnetic/radio frequency interference shielding [5], strain sensors [6], microwave applications [7] or electrostatic discharge materials and coatings [8].

1.1 Electrically Conductive Adhesives

Electrically Conductive Adhesives (ECAs) are based on creating a percolation pathway, a conductive bridge from one point of the surface on the ECA to another, by conductive filler particles in a polymer matrix. The conductive particles may be very different from each ECA to another, but the most used are silver, aluminium, gold and copper [9].

To achieve a conductive pathway, there have generally been two approaches to accomplish this. The first approach is to fill a polymer with the conductive filled material up to a concentration where there is a continuous pathway throughout the composite, and is called an Isotropic Conductive Adhesive (ICA) [4]. The other approach is to use particles with a diameter larger than the composite width in the conducting direction, and is called an Anisotropic Conductive Adhesive (ACA) [4].

Lately a third class of ECAs have been investigated, namely the aligned Anisotropic Conductive Adhesives. Such adhesives are based on using a low fraction of filler particles much smaller than the composite which are aligned to form conductive bridges from one side of the composite to the other by either an electric or magnetic field. The resulting conducting wires throughout the matrix appears quasi- one dimensional.
The class offers exciting opportunities as the properties of the composite depends strongly on the filler particles, and may show interesting specifications both with regards to conductivity and mechanics.
A fundamental property of using aligned ACAs is that the volume fraction of filler material of these composites is much lower than that of other ECAs, but with lower conductivity. The reduced material costs from lower concentrations are particularly interesting with regards to low dimensional applications like electrostatic discharge applications [8].

1.2 Carbon Nanocones and Disks

Carbon structures have been investigated thoroughly the last decades as the four forms; graphite, diamond, fullerenes and lately the carbon nanotubes (CNTs).
In the last years a new form of carbon structures has been in the spotlight, namely the carbon nanocones (CNCs). Carbon cones and disks are structures of carbon which are considered a fifth carbon form in addition to the previously known. The CNCs should not be confused with nanohorns [10], conical crystals of graphite [11] or naturally occurring helically wound graphene sheets [12], the CNCs are seamless at the wall and is grown by some other mechanism not fully understood yet [13].

The structures are often simply called CNCs, while strictly speaking; the term includes both cones and disks.

The first reported carbon nanocone to be synthesized was published in 1966, and was the corannulene molecule which is a carbon structure with a single pentagon at the tip [14]. The theoretical existence of other CNCs was later published in 1994 [15], and another class of carbon nanocones were synthesized shortly after the same year. This revealed graphene cones and cone-shaped fullerenes, but still with only one fixed apex angle and of very small quantities [16]. In 1997 there was a breakthrough, as CNCs of all apex angles were synthesized in large quantities [17] by the Kvaerner Carbon Black and Hydrogen process (CB&H) [18]. The diversity in cones is unique for the process, and has enabled the modern studies of CNCs.

1.3 Earlier Work

1.3.1 Aligned Anisotropic Conductive Polymer/Carbon Nanocone Adhesives

Aligned Anisotropic Conductive Adhesives have earlier been synthesized and published using a lot of different resins and filler materials like metallic particles [19], carbon black [20], carbon fibres [21] or carbon nanotubes [22]. When it comes to systems using (CNCs) as filler material, the first reported alignment was published in 2007, but then as a study of complex fluid of aligned CNCs in silicon oil [23]. This work presented how CNC particles may form chains while subjected to an AC electric field, with as low as 50 V/mm field strength. While the alignment was reported, the focus of this article did not involve conductivity enhancement, but rather the effects in the electrorheological fluid.
In 2010, a paper on aligned CNCs in a polymer composite was published, documenting how similar chains of CNCs may form in polymer dispersions [8], with methods based on the research on similar composites using single-wall CNTs [24]. The dispersions were reported to be fixed after curing, so that the composite had increased conductivity after alignment and curing compared to before. It was reported that conductivity in the aligned

ACA was up to 3-4 orders of magnitudes higher than the same fraction (0.2 vol %) composite without alignment. Around the same time, it was reported how the same composite could realign if the aligned CNCs were damaged before curing, by extending the alignment time [2]. The polymer/CNC composite was in 2011 reported to have interesting applications with regards to strain sensors [6], utilizing the variation in conductivity when a carbon string is stretched.

1.3.2 Present Problems in the Field

While there have been extensive reports and investigations on the properties of aligned ACAs in optical microscopy, SEM, AFM, SPM and other tools to investigate macroscopic structure, conductivity and change to parameter settings, there is still very little knowledge of the inner structure of aligned anisotropic conductive adhesives.
In aligned anisotropic conductive adhesives there are many questions which have not been answered. How does the contact interface between each particles look, is it a point contact or a larger overlap? How are the particles distributed at the electrode surface, and what is the contact interface between electrode and particles? Such questions will need to be addressed to fully understand the mechanics of the composite class.

Since several of the questions will need to be addressed at a nanometre level, they also require a nano tool to investigate them. High spatial resolution transmission electron microscopy is a good candidate to solve such problems, as long as a good sample preparation routes are accessible.
There are several problems with creating such a sample, where the first arise from the nature of the composite class. Since these composites are not isotropic, the particles will not be distributed homogenously in the sample. This creates a problem in a volume specific sample preparation method where the target area is not controllable. In such a method, there is a chance that the sample do not show the information required.
A second problem arises if hard particles are fixated in a comparably soft polymer. Any mechanical tool which may come in contact with a particle may dislocate particles, which could lead to destruction of the polymer in the vicinity.

The third problem which may arise is completely specific to the polymer, and that is the interaction between the polymer and any external chemicals, or heat, which are both normal to use in a TEM preparation environment.

1.4 Project Definition

To increase the understanding of aligned ACAs, the work described in this thesis was aimed at trying to answer fundamental questions about the inner structure of aligned polymer/CNC composites.
The main problem in the work was to search for and establish a working sample preparation method for TEM to investigate the interfaces between aligned CNCs in the composite. Other questions were also to be investigated by the method, such as discovering the creeping properties of the polymer around the CNCs to check if the polymer creates cavities around the particles or completely surrounds them.
Another TEM sample preparation technique was also to be established to investigate the interface between electrodes and particles.

In addition, a sample preparation method to investigate polymer wetting onto the particle surfaces would be established and investigated.

General scientific curiosity also demands more information about carbon nanocones, which still have a lot of questions unanswered.
Already known methods to prepare TEM samples to study CNCs will be utilized to answer selected basic questions of CNC morphology such as tip and wall-edge structure, and progress in investigation of how large the basic structural units of graphitized CNCs are.

2. Methods and Theory

2.1 Carbon Nanocones and Disks

A mathematically perfect single-wall carbon nanocone (SWCNC) may be realized as a circular single graphene layer which is modified so that a 60° zone is removed, and then the dangling ends are adjoined. Figure 2.1–1 illustrates the concept and how the new structure gets an apex angle of 112.6° with a single pentagon at the tip.

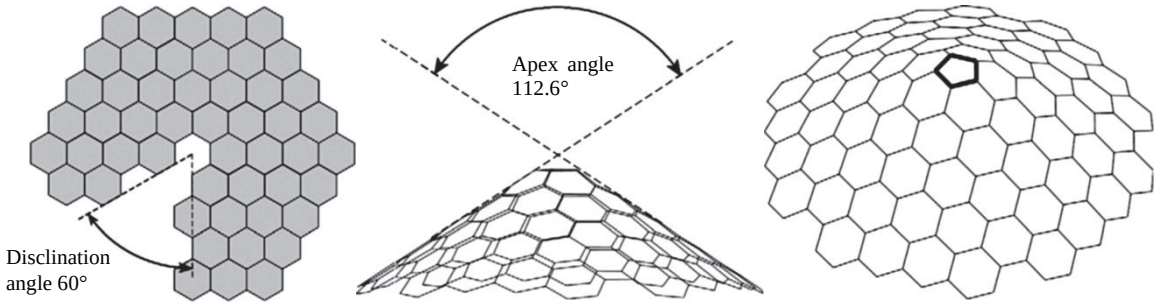

Figure 2.1–1: Formation of a cone from a graphene sheet with disclination angle of 60°[1].

The removal of such a zone may be multiplied, so that the sections removed may equal **n** x 60°, up to the maximum **n** = 5. The integer **n** multiplied by the sector size describes the disclination angle which is the removed area, and corresponds to a crystallographic line defect [1].

The structure created by **n** = 0 can be regarded as a carbon disk, while the remaining 5 structures each create cones with various discrete apex angles as shown in Table 2.1-1. Each representation of a SWCNC has a different tip structure, consisting of a symmetric combination of pentagons mixed into the hexagonal mesh. It is still not clear if the structure seed starts with the pentagon defects, or if they are just a product of the structure formation.

Table 2.1-1: The theoretical apex angles of SWCNCs and the corresponding number of pentagons at the tip.

n	Disclination angle	Apex angle	# of pentagons
0	0°	180°	0
1	60°	112.9°	1
2	120°	83.9°	2
3	180°	60.0°	3
4	240°	38.9°	4
5	300°	19.2°	5

In reality, CNCs have not yet been reported to be occurring in a SWCNC form, they rather form as layered structures of semi-amorphous material, with reported layers of approximately 100-150 layers [25]. The core is made up of fairly uniform graphitic layers and as one approach the outer layers the structure turns increasingly amorphous, while still keeping some sort of layered structure. This corresponds with how carbon black has been reported earlier, as organized small area layers and grains generating an overall semi-layered structure [26, 27].

While the above mentioned cones represent the CNCs which are the easiest to visualize, cones may have a broad range of apex angles and structures.
Studies of CNCs from one synthesis route [17] reported that the apex angles can actually be viewed as a distribution, where the cones of **n** = 1 to 5 only show the peaks in the distribution. The non-discrete apex angle cones have a non-symmetric pentagon pattern at the tip [1].
CNCs may also have more than one tip, or any other tip variation previously described in a multitude of publications [28, 29].

2.1.1 The Discovery from the CB&H Pyrolysis

In 1997 it was discovered that at special conditions, only about 10 % of the output of the Kvaerner Carbon Black and Hydrogen Process (CB&H) [18] was in fact carbon black

[17]. The CB&H process is a zero-emission pyrolytic process which decomposes hydrocarbons directly into carbons and hydrogen by using a plasma torch with temperature above 2000°C.
The product mentioned was discovered to be large quantities of CNCs, where about 70% of the total product was disks, about 20% was cones, while only 10% was traditional carbon black. Studies of the material showed that while the product contained cones with apex angles consistent with structures of 1 to 5 pentagons at tip end, a great structural diversity was exhibited, originating from various defects.

2.1.2 Graphitization of Carbon Nanocones

The graphitization of CNCs is usually performed by heat treatment under a noble gas like Argon at up to 2700°C, which studies of CNCs have shown gives well defined layers.
Previous studies have shown that CNCs graphitize by heat treatment, ordering the layers from semi-amorphous outer shell, to highly regular layers throughout the particle [30].
For such a transformation to occur, Oberlin and co-workers [26] concludes that this must mean the carbonaceous material must be made initially of small Basic Structural Units (BSU), which are small sheets or grains of semi-amorphous grains of less than 10 Å in size. Additionally, these BSUs must align approximately parallel in large areas.

The wall structure of non-heat treated CNCs is a combination of crystalline material and close to amorphous domains, discovered by diffraction pattern. After heat treatment diffraction has shown sharp rings, with several sets of spots with six-fold symmetry. This have been interpreted so that the amorphous part of the particle is graphitized into graphene-like sheets stacked on top of each other with similar tilt of all the sheets in the x,y-plane [13].

2.2 Electrically Conductive Adhesives

Electronically Conductive Adhesives (ECAs) are composites of polymer and a conductive filler material. Such composites are commonly used to replace the lead-tin

soldering alloys for electronic packaging and interconnections, but are also applicable to numerous other applications.

Conduction in these composites is generally achieved by creating a conducting bridge from one point on the surface of the composite, to another point. This can be done either isotropically or anisotropically.

2.2.1 Isotropic Conductive Adhesives

Isotropic Conductive Adhesives (ICAs) are the most common of the ECAs, and the simplest. The conducting path occurs when the fill-ratio of the conductive particles are increased above a point where conducting pathways are formed from one of the outer sides of the matrix to the opposing by random pathway. This fill-grade is called the percolation threshold and follows the laws of percolation theory, and varies depending on the filler material. Conductive fillers include silver (Ag), gold (Au), nickel (Ni), copper (Cu) and Sn, SnBi or SnIn coated Cu in various sizes and shapes [31]. Ag is the most common conductive filler for an ICA due to its high conductivity, but the cost is a major drawback for wide use. The advantage of ICAs is that there is always a multitude of pathways for conduction, so conductive properties are likely to uphold even after an event of mechanical stress. Because conduction is achieved by a high particle fill grade, ICAs often have decreased inherent polymer properties like sheer strength and flexibility, which may be critical in certain applications.

2.2.2 Anisotropic Conductive Adhesives

Anisotropic Conductive Adhesives (ACAs) is a fundamentally different approach to ECAs than ICAs. In such an ACAs, the goal is to create semi-controlled conducting pathways through the composite in only one dimension.
This is achieved by one of two methods, where one of them is to use conducting particles which are equal or larger in size than the width of the composite in the conducting direction. The other method is to use small conducting particles compared to width of the

composite, which are aligned in strings by either an electric or magnetic field. These chains of particles form conducting pathways like for ICAs, except that there is no system wide three-dimensional network, the conductivity increase compared to only polymer only applies in the direction of the electric or magnetic field, or perpendicular to the surface for non-aligned ACAs. The maximum conductivity is generally lower than a typical ICA, but a much lower fill-grade is needed to obtain conductivity. The advantage of this property is that the total cost of the conducting particles may be lowered, and also the composite keep most of its inherent polymer properties.

2.2.2.1 Aligned Anisotropic Conductive Adhesives by Dielectrophoresis

As mentioned in section 2.2.2, aligned small particle ACAs can generally be aligned by a magnetic or electric field. When using an electric field and charge-neutral particles, the particles are moved by dielectrophoresis (DEP) [32]. DEP works for electric fields induced by either AC or DC voltage. There are some advantages by using AC over DC, one being that any ions in the system will not be moved by DEP. Another advantage is that the method prevents the creation of Debye screening layers at the electrodes [33].

While using DEP in a field induced by an external AC source and non-polar particles, at each point in time there is a specific field strength and direction between the electrodes. This field will then polarize the particles within the field, and create local fields around these particles which are symmetric around the field direction. The field from the particles will be partially shadowing the external field, so that the net sum of fields will be non-homogenous between the electrodes. The particles will have a higher field gradient in the direction of the alignment, so the particles can join up into quasi one-dimensional chains, which create the phenomena of electric-field induced assembly.

Alignment of such composites depends strongly on the dielectric constant of the particles and the polymer, as well as the strength and frequency of the AC field [34]. The polymer base type may also influence alignment and chain formation [35].

2.3 Transmission Electron Microscopy

Transmission Electron Microscopy (TEM) is a tool for nano- and micro- metre scale studies of solid materials using electrons as probing unit. The method is much like visible light microscopy, but since the minimum wavelength of visible light (λ = 400nm) is so much higher than for electrons (λ = 0.0251nm for 200kV TEM), the theoretical resolution of TEM is orders of magnitude higher than that of the visible light microscope. An advantage of the TEM is the possibility to do diffraction, imaging and spectroscopy in the same instrument, while still being able to move and tilt the sample.

A TEM is a complex system which starts in the end of a vacuum column where there is an electron gun accelerating electrons to the required voltage of the system. The electron gun emits electrons from either a LaB_6 or a Tungsten hairpin filament, or by a Field Emission Gun (FEG), and the electrons are then accelerated in the sample direction by applying a large bias on the anode. The bias of the anode equals the energy of the electrons.

The accelerated electrons travel down the column and through a series of apertures and electromagnetic lenses, before hitting the sample. The transmission of electrons through the sample generates a variety of signals which can be measured and quantified using various techniques. The most common signal to use is the transmitted electrons or x-rays. Electrons transmitted through the sample can be observed on a phosphorous screen generating visible light from the electrons hitting the plate, or by using a camera situated behind the screen.

The illumination system, the system which controls the beam from the gun onto the sample, influences the beam by adjusting apertures and the current through electromagnetic lenses and deflection coils. The projection system controls the beam from the sample down to the phosphorous screen.
Apertures adjust the intensity, contrast and area selection onto the screen, while the lenses in the system mainly adjust the focus and spot size illuminating the sample. The

deflection coils enables tilt and shift of the beam. An overview of the system is shown as an illustration in Figure 2.3–1.

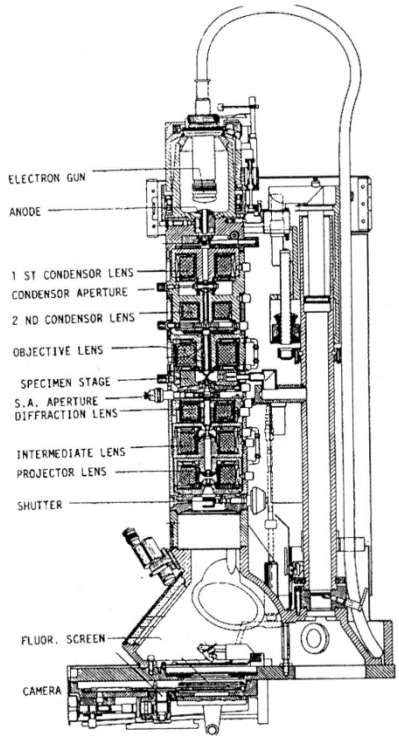

Figure 2.3–1: Illustration cross-section of the main components of a TEM [36].

A TEM is designed to be able to operate in both diffraction and imaging modes while using transmitted electrons. In imaging mode, all electrons from one point in the sample are imaged onto the viewing screen to create a real space image of the sample, and the image plane is observed. In diffraction mode, all electrons which are scattered at the same angle by the sample are converging at the same points at the viewing screen, where the diffraction plane is observed. Figure 2.3–2 shows a simplified ray diagram of the beam paths in TEM, and illustrates how the imaging and diffraction modes correspond.

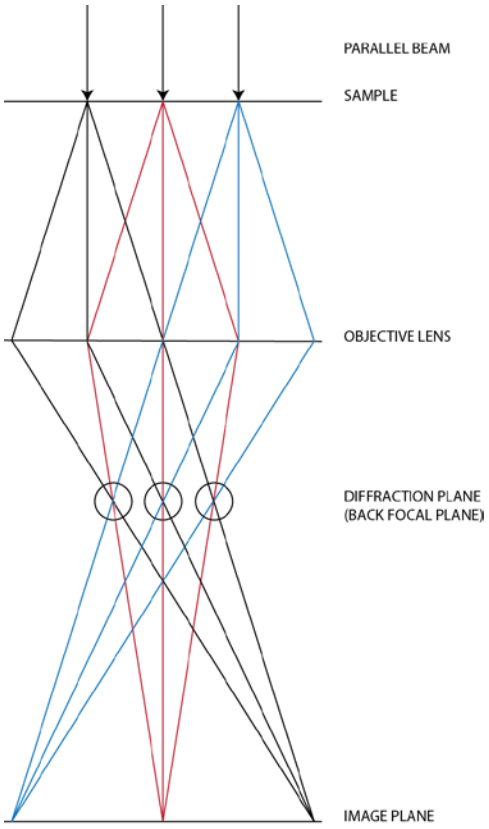

Figure 2.3–2: Simplified ray-diagram in a transmission electron microscope.

2.3.1 Imaging in TEM

Imaging in TEM is utilized by focusing the image plane onto the phosphorous screen, or to the camera behind. In the resulting image, contrast dominates the information which can be interpreted. Brightness in TEM is only a property of the electron gun and the beam angle, and does not contribute to information. Beam intensity can be moderated by the use of a condenser aperture which limits the beam, and the spot size which illuminates the sample can be adjusted by the condenser lens.

While contrast in visible light microscopy arises from absorption of light in the sample, contrast in TEM arises from scattering of the beam in the sample. The transmitted electron can have both its amplitude and phase contrast changed by this scattering, and both gives contrast on the screen. Therefore, contrast is divided into both amplitude contrast and phase contrast, which is in important distinction. Although the electron

changes both amplitude and phase in all samples, amplitude contrast dominates TEM imaging at lower magnifications.

Amplitude contrast arise from variations in mass, thickness or local variation in diffraction of the sample and are generally divided into two categories, mass thickness contrast and diffraction contrast [37]. The major difference is that the mechanics of mass-thickness is caused by incoherent scattering, while diffraction contrast arises from coherent scattering.

Mass thickness contrast is caused by Rutherford scattering, and is contributed by both the atomic number Z, and the thickness of the sample. In a conventional TEM at bright field imaging, this is the predominant contrast mechanism, where changes in mass and constituents in two given points give rise to contrast in the picture.

Diffraction contrast in TEM is caused by fulfilment of the Bragg condition in the given angle to the planes of the sample.

Amplitude contrast can be used and manipulated in many different ways, but the easiest methods are Bright Field (BF) and Dark Field (DF) imaging. In a BF image, the direct beam is allowed to pass through the aperture in the back focal plane. A DF image is formed if only scattered electrons are passed through the same aperture [36].

2.3.2 High Resolution Transmission Electron Microscopy

In High Resolution Transmission Electron Microscopy (HRTEM), a large objective aperture is used so that several diffracted beams contribute to the image [36]. By using the method, a very large information set is transferred to the phosphorous screen.

Unlike low resolution TEM which can be simplified as the Rayleigh criterion to distinguish two objects, HRTEM resolution limits are governed by phase transfers.

To achieve maximum resolution in a specific microscope, the goal is to transmit as many beams as possible through the illumination system with the same phase, which means a large coherent beam area [37].

2.3.3 Bragg's Law

The double slit experiment is a visible and well-known phenomenon in physics, where a planar wave hits parallel slits and the wave property of the photons generates constructive interference. Bragg's law is based on the equivalent wave property of electrons and x-rays illuminating a sample. A plane wave incident to a family of lattice planes will be scattered, and will at a certain condition cause constructive interference, namely the Bragg condition. This is illustrated in Figure 2.3–3.

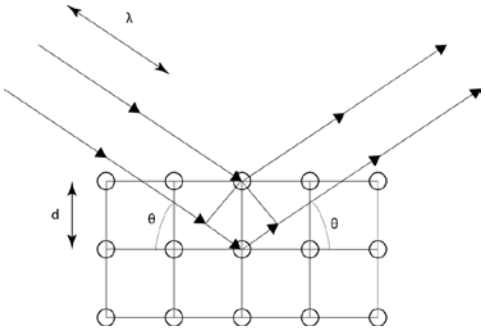

Figure 2.3–3: Illustration of Braggs law. Bragg's condition is satisfied when $n\lambda = 2dsin(\theta)$.

The condition for constructive interference is that at for the certain angle θ, the phase must be equal to that of the parallel probing unit. By simple trigonometry, this gives the following requirement for coherent scattering from the crystal lattice:

$$n\lambda = 2dsin(\theta), \quad \text{(Equation 1)}$$

which is Bragg's law.

Bragg's law and its diffraction equivalent can be applied to kinematic conditions in diffraction mode, and diffraction contrast in imaging.

2.3.4 Diffraction

Electrons transmitted through the TEM are scattered by the nucleus and electrons during transmission through the sample. The electrons can be scattered both kinematically and dynamically, each describing different events. Kinematic scattering takes into account direct scattering from the beam, and the electrons are scattered in a single direction in a

small angle away from the optical axis. Such events may fulfil Bragg's law, so that electron waves are in phase and cause interference.
Such interference gives rise to interference patters, or diffraction patterns.
Dynamical scattering is the theory used to describe the information from already scattered beams interacting with the sample yet again.

2.3.4.1 Selected Area Diffraction

Selected area diffraction (SAD) is a method to utilize the properties of diffraction to transfer information about the crystal structures of a given area. In the method a parallel beam is used, and an aperture is inserted in the image plane so that only signal from the selected area is considered in the viewing screen.
The diffraction pattern shown in the viewing screen is then a two-dimensional projection of the reciprocal space perpendicular to the beam.

2.4 Sample Preparation for Transmission Electron Microscopy

As TEM imaging is based on transmission of electrons through a sample, the samples need to be very thin to minimize absorption. This is necessary to have a good intensity and contrast in imaging mode, and to minimize multiple scattering to approach kinematic conditions in diffraction mode. The thickness of TEM prepared samples are normally in the range of < 100 nm, depending on atomic number of the elements in the sample and the acceleration voltage.
With a bulk sample which you do not want to crush or dissolve, the routes to achieve a stable sample which is thin enough are generally either to cut nanometre slices by ultramicrotomy, or by mechanical abrasion like surface- and/or dimple- grinding combined with ion milling or electropolishing.

2.4.1 Cryo- and Ambient-Ultramicrotomy

Ultramicrotomy is a method for obtaining thin slices on the nano- or micro- meter scale, by cutting a sample with a very fine and specialized knife, at room temperature [38]. This

is performed with a microtome which holds the knife in place, and the sample is tilted and moved in three dimensions in order to cut the sample.
Cryoultramicrotomy follows the same principles, but cutting is done in cryogenic temperatures using liquid nitrogen. The advantage of microtomy in cryo temperatures is that otherwise soft materials which are hard to cut well due to interaction with itself or equipment are hardened enough to be cut successfully.

Before a good cut is obtained the sample needs to be trimmed. The face of the sample is cut into a shape which provides the least force on the knife, reducing the wear and tear on the knife, and resulting in the best possible slice with a minimum of flaws and distortions. These trimming cuts are normally done with a knife of a lesser quality than the knife for the final cuts. Thicknesses of cuts are usually decided by reflection colour.

Sectioning can be performed as both dry and wet sectioning at room temperature, but wet sectioning in cryoultramicrotomy is only possible with semi-elevated temperatures. In wet sectioning a special knife truf is used, illustrated in Figure 2.4–1.

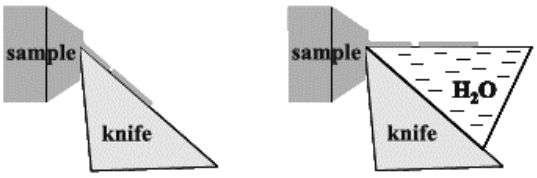

Figure 2.4–1: Dry and wet sectioning [38].

Wet sectioning is less harmful to the slices, as the sections are floating freely on the water by surface tension. In dry sectioning, there is an increased possibility that the sections are curled up or destroyed by tension and friction towards the blade of the knife.

3. Experimental

The following sections contain information and explanation regarding the methods, equipment and chemicals used. All CNCs used in the experiments were already heat-treated at 2700°C under Argon gas for three hours, and supplied by n-Tec, Norway.

3.1 Preparation and Alignment of Polymer/Carbon Nanocone Composites

To create the composites, CNCs and polymer in various ratios was mixed by using a magnet stirrer for 20 minutes, with a stir speed of 50 rpm to avoid excess air-bubbles. After this stirring time, the dispersion was reasonably uniform, with reported dispersed particle size <10 μm, containing a few CNCs [2]. When using UV-curable polymer, simple light shielding like aluminium foil was used to avoid partial curing and increased viscosity. No detergents, sonication, or vacuum-pump was needed.
The polymers used in the samples were the UV-curable Dymax 3094 STD or Dymax See-Cure 1201-M-SC, the two-component Huntsman Araldite AY 105-1 with amine hardener Ren HY 5162 mixed by 2:1 per weight, or by mixing resin Gatan G1 with hardener Gatan G2 mixed by 10:1 per volume.

After creating the dispersion, the samples were aligned by an electric field. The field was generated by either a custom-made AC source, or by a BK Precision 2MHz Function Generator 2010A with a Trek High Voltage Amplifier Model 2210. The frequency was set to 1 kHz for both setups, while the voltage was sample specific. Alignment of the particles for a CNC-composite was performed in two different ways, either by in-plane, or out-of-plane alignment.

While the electric field was maintained, the polymer was cured by using ambient conditions for the Huntsman Araldite, heating plate for the Gatan G1, or a UV-lamp for the Dymax 3094 and Dymax See-Cure

Table 3.1-1: Table of aligned samples.

Sample ID	Polymer system	Vol % CNC	Field Strength	Alignment
Sample A	Gatan G1	0,20% vol	0,55 kV/cm	In-plane
Sample B	Dymax 3094	0,12% vol	0,91 V/cm	In-plane
Sample C	Huntsman 105-1	0,30% vol	2,75 kV/cm	In-plane
Sample D	Dymax 3094	0,24% vol	1,50 kV/cm	Out-of-plane

3.1.1 Out-of-Plane E-field Alignment

In order to create samples which were aligned out-of-plane, a dispersion of CNC-material in polymer was dripped onto the conducting side of an electrically conducting glass-plate. The glass was a tin indium oxide (ITO) covered glass plate, which was cut into pieces matching the experiment by using a diamond pen and breaking technique. Using scotch tape as spacing, a second piece of conducing glass was placed with the conducting side towards the polymer and CNCs mix. To each conducting surface, a wire was connected, fastened by a commercial silver particle conducting adhesive. An illustration of the setup is shown in Figure 3.1–1.

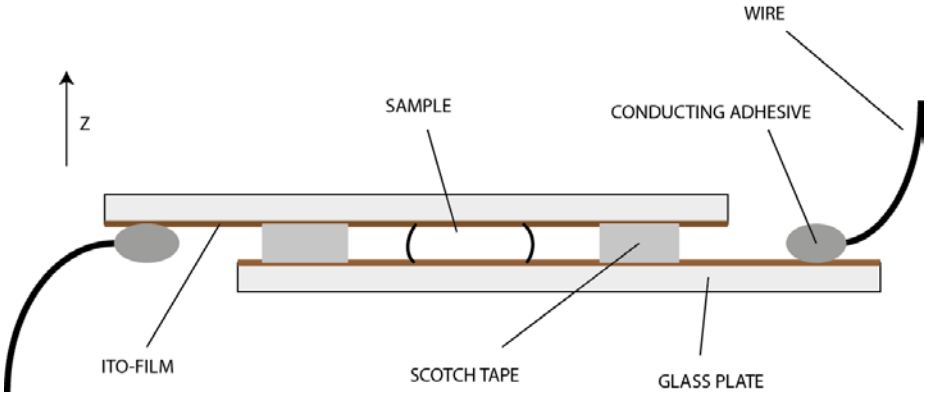

Figure 3.1–1: Illustration of out-of-plane alignment setup. A CNC in polymer dispersion is put between two conducting surfaces, which act as the electrodes for alignment. The wires are connected to an external power supply.

An AC-current was then applied to the wires, aligning the particles in the mix by DEP. With the AC-field maintained, the polymer was cured.

Alignment was confirmed by measuring resistance between the two conducting glass plates. After curing, wires were detached, and one of the glass plates was carefully pulled off by use of hands and a scalpel.

3.1.2 In-plane E-field Alignment

In-plane E-field samples were created by first making a template. This was made by gluing two parallel pieces of metal to the surface of a microscope slide, using commercial contact glue. The metal used was aluminium or copper plates, cut to strips, flattened coarsely by a clamping tool, and grinded slightly with a rough grinding paper to increase connectivity with the glue and level the surface. Each metal piece was added a wire, glued in place by a commercial silver particle conducting adhesive.

The gap between the metal pieces was closed at both ends with contact glue, to contain the mixture. An illustration of the template is shown in Figure 3.1–2.

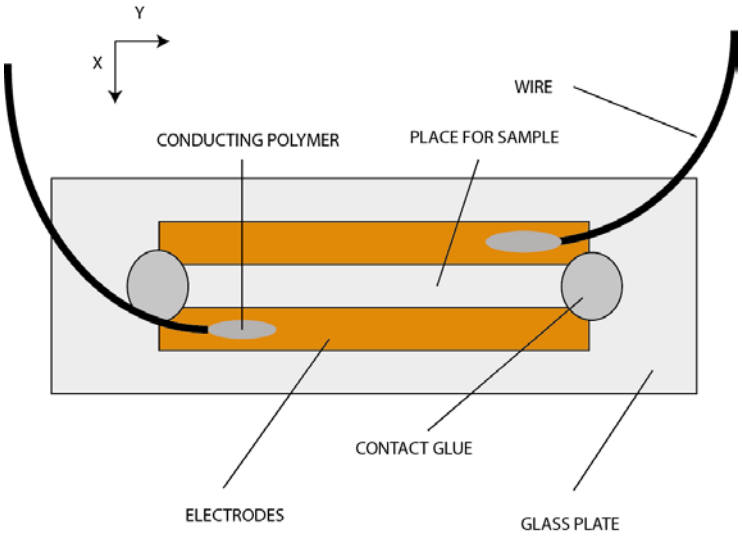

Figure 3.1–2: Illustration of template for in-plane alignment. A CNC in polymer dispersion is filled in the space surrounded by the electrodes and the confining contact glue. The wires are connected to an external power supply.

Using this template, a CNC and polymer dispersion was dripped into the slit between the metal strips, and an electric field induced by AC power-supply was applied. With the AC-field maintained, the polymer was cured. The alignment and curing were performed

under a light-microscope to check for alignment in-situ, except for the use of Gatan G1 resin where the sample was moved to a heating plate for curing.
Alignment was confirmed visually by light microscopy, and by measuring resistance between the metal strips for the thick samples.
The sample was removed from the template by removing the metal strips, and then removing the composite from the template with a scalpel. The template was not reusable after synthesis of one sample.

3.2 Sample Preparation for Transmission Electron Microscopy

The following sections describes in detail the different methods used for TEM sample preparation. In Table 3.1-1, the various TEM samples shown in section 4 and 5 are presented.

Table 3.2-1: Table of TEM samples. Sample ID is reference to Table 2.4.4 1.

Preparation ID	Prepared From	Preparation Method
Sample 1	CNCs	Dispersion on grid
Sample 2	CNCs and Polymer	Dispersion on grid
Sample 3	Sample A	Grinding and ion milling
Sample 4	Sample B	Matrix-embedding and ion milling
Sample 5	Sample C	Cryo-ultramicrotomy
Sample 6	Sample D	Cross-section

All grinding were performed using various grit SiC Paper from Struers.

3.2.1 Dispersion on Grid

To prepare sample 1 for investigation of CNCs by TEM, CNC-material was dispersed in ethanol and sonicated with a Branson Ultrasonic 2200 for 2 minutes to ensure a reasonable dispersion of particles. A single drop of the dispersion was left on a Holey Carbon Grid from Agar, laying on a filter paper. The standard method to do this is to let

the grid hang free using a tweezer. However, the reason to change this was to reduce the drying time, and to decrease surface piling due to the drying conditions. With a shorter drying time the carbon is assumed to be distributed more evenly on the grid.

Sample 2 was prepared in a similar way as sample 1, but in addition a UV-curable polymer Dymax See-Cure was added to the ethanol and CNC after sonication. The polymer has the properties that it is coloured blue, changes colour after curing and is soluble in ethanol. The colour property of the polymer makes the curing time visible. The polymer used was out of date; however the curing was a posteriori shown to be adequate.
Curing and drying of dispersion was done overnight underneath a standard table-lamp, at ambient temperature.

3.2.2 Cryo- and Ambient-Ultramicrotomy

Ambient Ultra-microtomy was performed with a Leica Ultracut UCT by securing the sample straight into the sample slot. The cuts were made with a basin with distilled water attached to the diamond knife, and slices picked up with a strand of hair connected to a plastic rod. The slices were put on Holey Carbon Grid from Agar.

Cryo-ultramicrotomy (Cryo-UM) was performed with a Leica Ultracut with a EM FCS cryochamber [39], using a customized sample holder. The standard aluminium sample-holder was drilled a hole with diameter of 0.6 mm and a depth of 4 mm.
The sample was inserted into the hole and added sucrose to secure it in place, before the sample was shaped and prepared for cut. An illustration of the modification and sample-securing for the holder is shown in Figure 3.2–1.

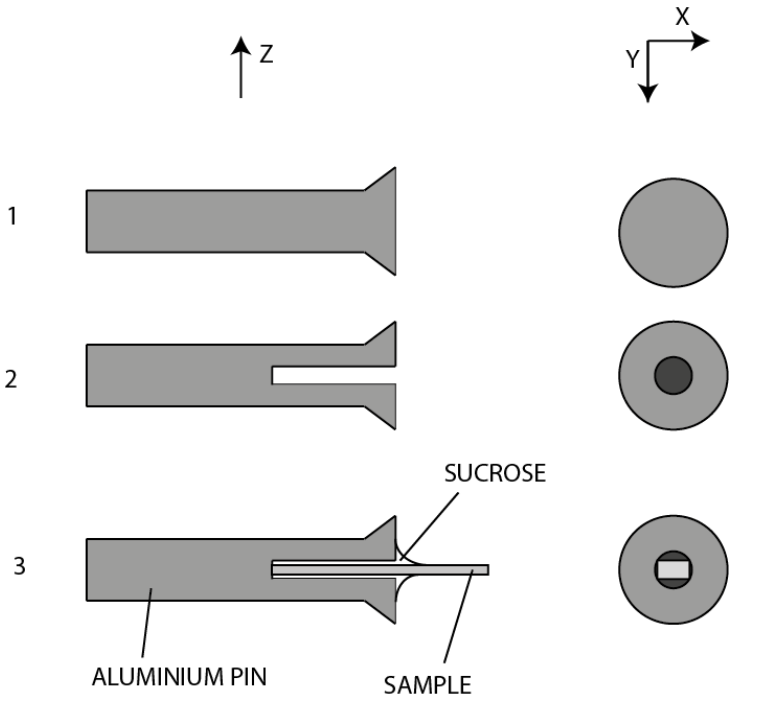

Figure 3.2–1: Illustration of sample-holder for Cryo-Ultramicrotomy

Cuts were performed in dry blade mode, and slices picked up by a strand of hair secured to a plastic rod, and the strand of hair moist with sucrose. The slices were put on Holey Carbon Grid from Agar.

Cutting in both modes were first trimmed by reducing the surface area of the sample to one that looks like a rectangular top of a pyramid, as illustrated in Figure 3.2–2., using a glass knife. Final cuts for slicing were done with a diamond knife.

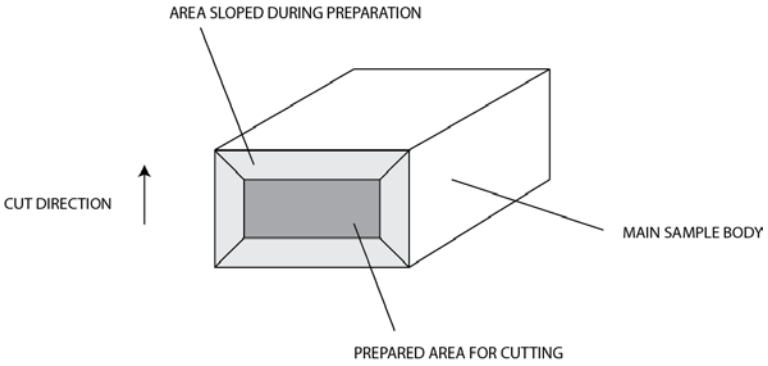

Figure 3.2–2: Illustration of sample prepared for cutting.

3.2.3 Matrix-embedded Cross-sections

Some samples were prepared by embedding an in-plane aligned sample in a brass tube with outer dimensions 3 mm x 3 mm, using the polymer M-Bond AE-10 by Micro-Measurement with M-Bond Type 10 hardener in as a matrix fill material. An illustration of the filled tube is presented in Figure 3.2–3.

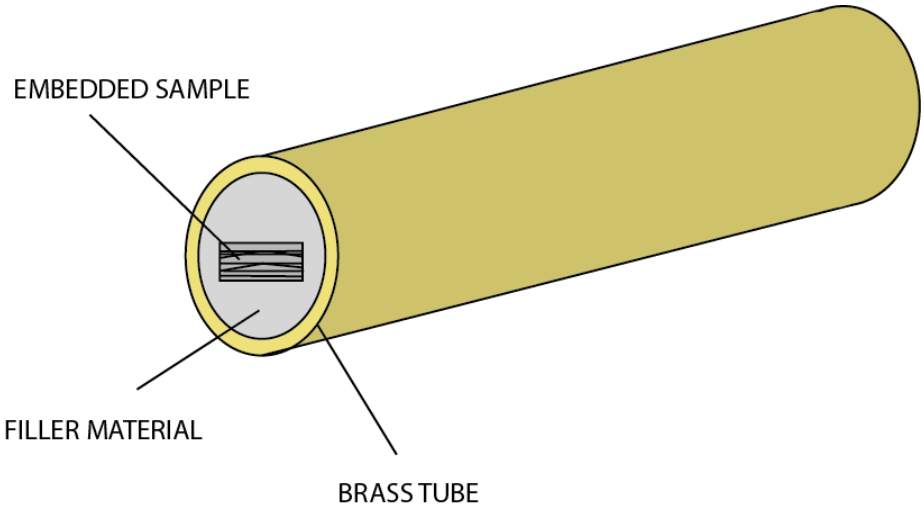

Figure 3.2–3: Illustration of matrix-embedded sample. The sample is embedded in a polymer filler material, inside of a brass tube.

The tube was then cut into 100 μm thin slices, with the cut perpendicular to the embedding direction. To cut the slices, a saw from Polaron Instruments with a SiC blade was used.

The cut slices was grinded by hand with no rotation with P1200 and P2400 grinding paper.

3.2.4 Grinding and Mounting

Grinding of material for thin TEM-slices were done by gluing the sample to a metal or glass support-rod with the polymer Crystal-Bond, which is hard at room temperature, and liquid at higher temperatures. Depending on hardness of sample, various grinding papers

were used, but always ending with P4000 for polishing paper before the next step. Thickness of the sample was chosen to be in the region of about 1 mm at this point.
The sample was then removed from the support rod on a heating plate, and washed in acetone followed by rinsing in distilled water. A 3 mm x 3 mm copper ring with inner dimensions of 2 mm x 1 mm from Agar was glued onto the grinded side of the sample, by using the resin Gatan G1 and hardener Gatan G2 with a mixing ratio of 10:1 per volume.
After reattachment of the sample to the support-rod, the side without the copper ring was grinded down to below 50μm with various grinding papers depending on sample. Grinding ended with using P4000 paper until final desired thickness.

3.2.5 Ion Milling

Ion milling of samples was performed using Gatan Precision Ion Polishing System Model 691 operating at 3.5 keV for matrix-embedded cross-section sample 4, and 4.5 keV for sample 3. For matrix-embedded cross-sections, gun angle was set to 4°Top/4°Bot to maximize the area of TEM inspection. For grinded samples the angle was set to 4°Top/7°Bot, increased angle at bottom gun was chosen to avoid sputtering copper from the copper ring onto the sample.
Holes were detected visually by back-lit sample and a microscope-mounted CCD camera.

3.2.6 Cross-sections

Cross-sections were made by cutting an out-of-plane sample which had not had the glass plates removed. The cut was done with a Microsaw by Technoorg Linda Ltd. with a cut perpendicular to the glass surface. The sample was then fixed to a support rod and grinded, as described in Section 3.2.4.

3.3 Electron Microscopy Investigation

The TEM investigation was done using JEOL 2000FX and JEOL 2010F analytical microscopes, both operating at 200kV. The JEOL 2000FX was equipped with a LaB_6 filament, while the JEOL 2010F was equipped with a FEG.

For both microscopes images and diffraction patterns was captured to Kodak Electron Microscope Film, developed on-site in a dark-room. Film was developed for five minutes in Kodak Professional Developer and then rinsed with water, followed by ten minutes in a solution of Tetanal Vario fixing salt and water. After fixation, the films were rinsed in running water for more than thirty minutes.

SEM investigation was done using a FEI Quanta 200 FEG-ESEM operating in High Vacuum mode. Investigation of TEM samples in SEM were done with a standard TEM to SEM sample holder.

4. Results

4.1 The Structure of Carbon Nanocones

In order to answer some fundamental question of CNCs, sample 1 was investigated by TEM BF imaging, and HRTEM.

4.1.1 Preliminary Investigation

To get a reference for subsequent experiments, basic CNCs in sample 1 were imaged in TEM by ethanol dispersion technique, and are presented in Figure 4.1–1. The images present the five various carbon nanocones with discrete apex angles.

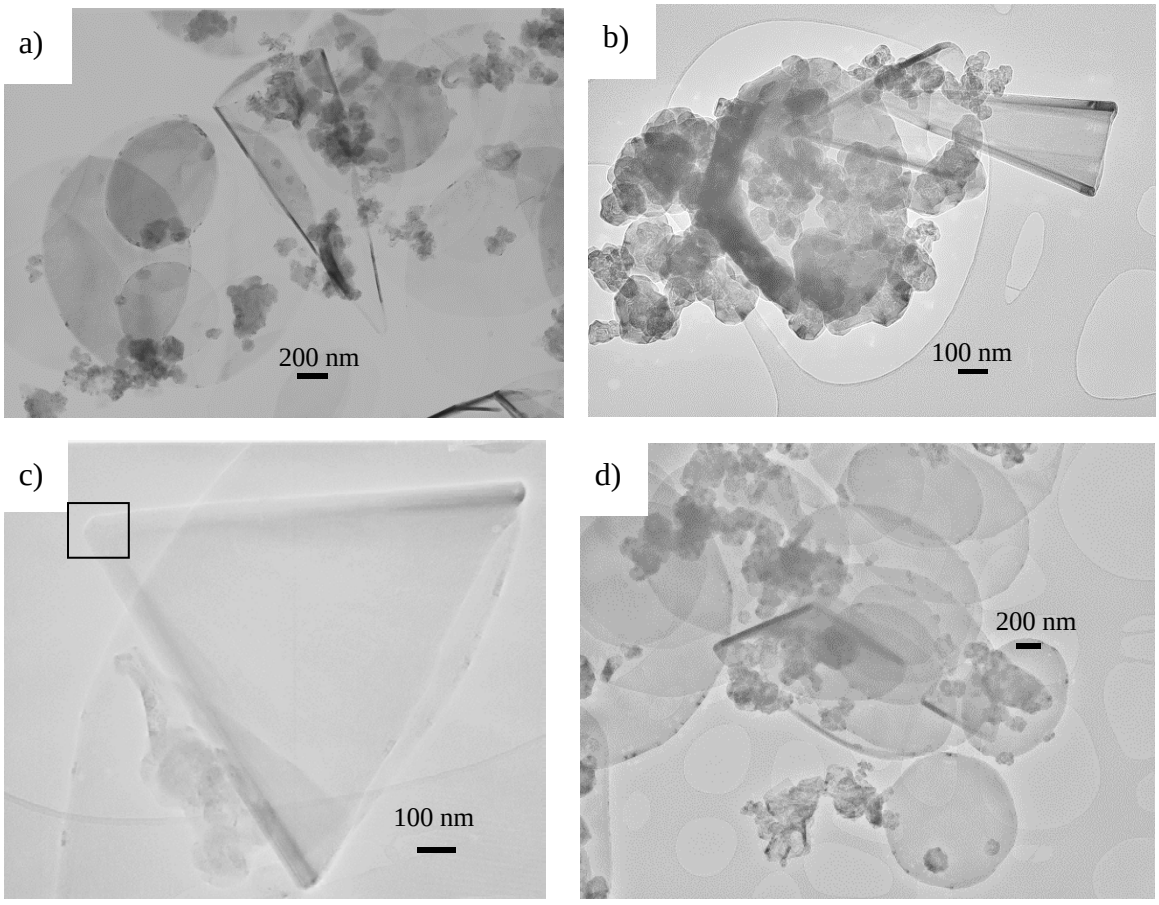

Figure 4.1–1: TEM images of carbon nanocones with various discrete apex angles. a) A CNC with apex angle α = 19.2° b) Three CNCs positioned in each other with apex angles α = 19.2°, 38.9° and 83.6° respectively. c) A CNC with apex angle α = 60.0°. d) A CNC with apex angle α = 112.9°.

The distribution of particle shapes and sizes complies with the previously reported; all the discrete apex angles of single-apex cones are shown.

Figure 4.1–2 a) shows typical carbon nanodisks.
An aspect which is worth mentioning is the distribution of CB particles on the disks. The image shows that while some disks have almost no such particles attached, others are completely covered with them. This indicates by itself that the CB particles are attached to the disks and not randomly attached by weak force interaction; otherwise the particles would've been distributed more randomly amongst the disks.

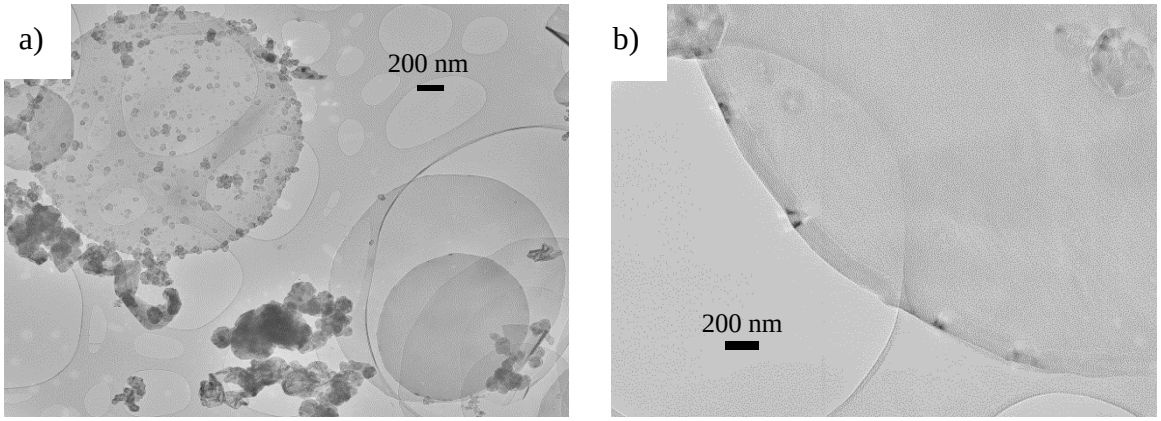

Figure 4.1–2: TEM images of carbon nanodisks. a) Disks with and without carbon black particles attached. b) The circumference of a disk, showing Bragg extinctions and reflections.

Figure 4.1–2 b) shows a magnified area of a disk where the rim shows dark regions. Since such regions are only visible at spread out locations, this indicates there is a non-uniform structure along the rim.

4.1.2 Circumferential Edge Structure

Figure 4.1–3 b) and d) are HRTEM images of a cross section view of the circumference of the disk in Figure 4.1–3 a) and a), investigated in order to discover the structure of the layers around the circumference of the CNCs. The images are from sample 1, prepared by ethanol dispersion.

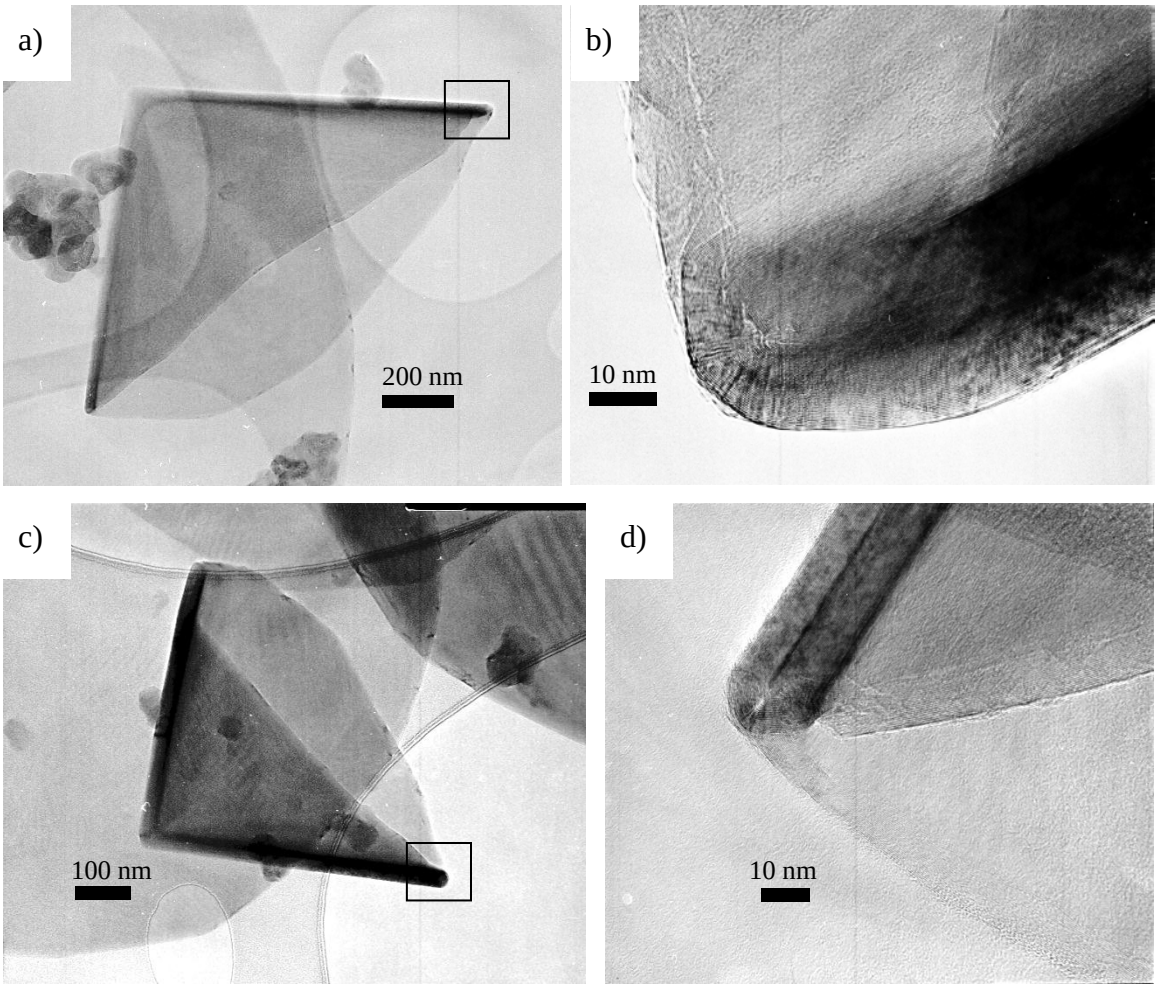

Figure 4.1–3: TEM image of a CNC. a) Overview image. b) HRTEM image of the CNC circumference cross-section. c) Overview image. d) HRTEM image of the CNC circumference cross-section.

Interestingly, the images show that the layers do not end at the circumference, and that the layer at the outside of the cone is the same as the layer on the inside, all layers are curled around an inner core which is in the middle between the innermost and outermost layers.

In the picture faceting of the layers around the circumference is also shown, and one can also see that other facets point out from the most dominant image layer.

The results from Figure 4.1–3 were data-mined by Fast-Fourier Transform (FFT) with results presented in Figure 4.1–4.

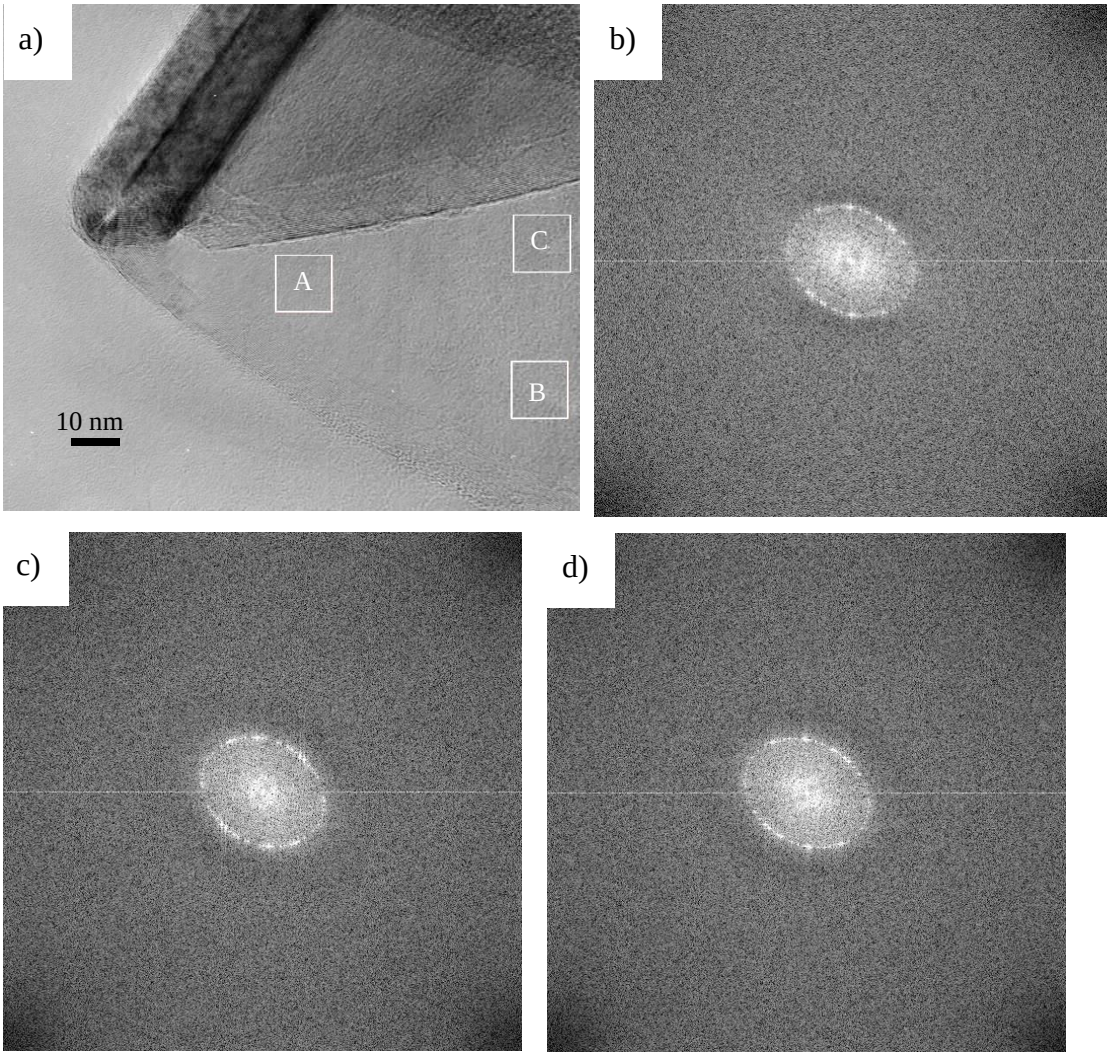

Figure 4.1–4: Fast Fourier Transform of a CNC wall. a) TEM BF overview image showing locations of FFT. b) FFT of location A. c) FFT of location B. d) FFT of location C.

4.1.3 Tip Structure

Figure 4.1–5 shows a CNC with a HRTEM image of the tip, which is representative for the CNCs observed.

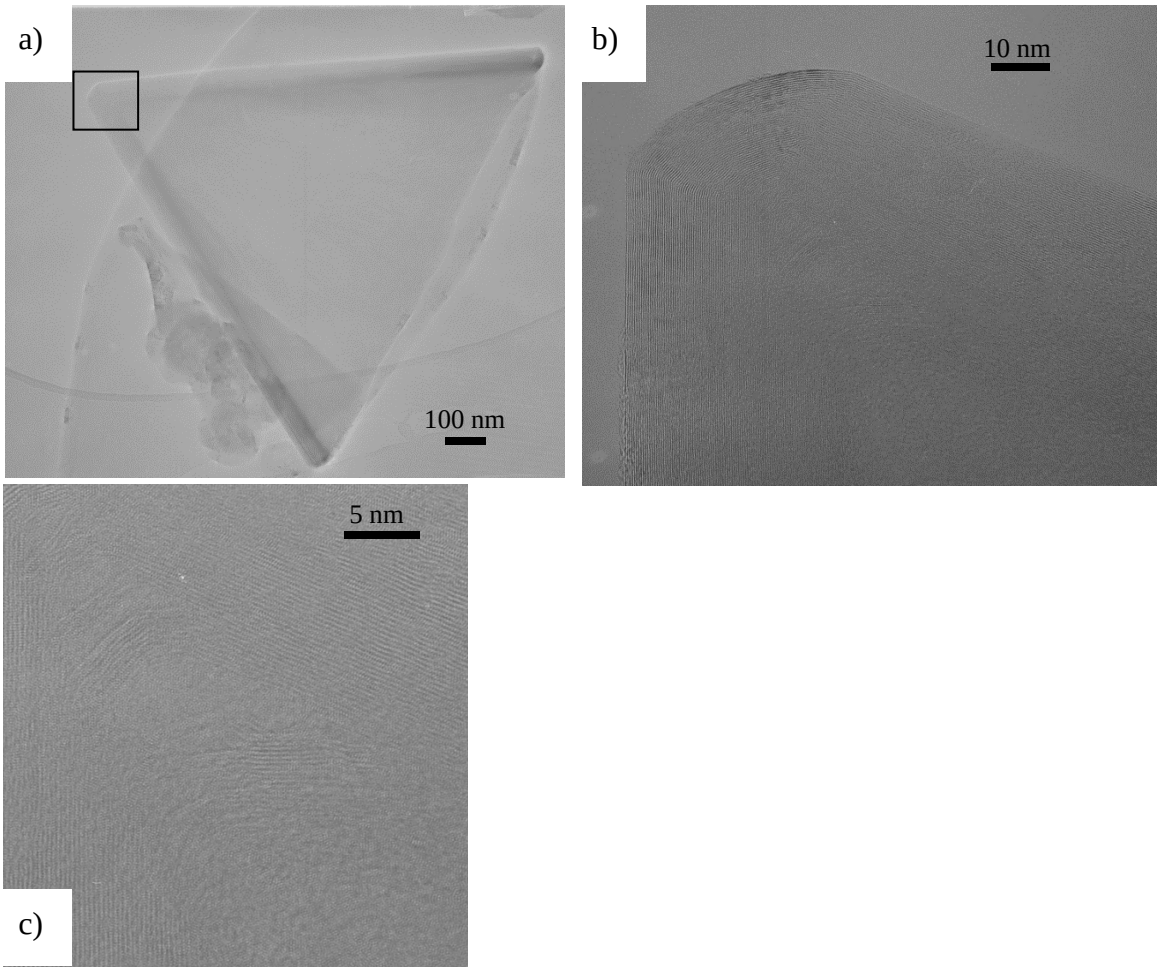

Figure 4.1–5: TEM image of a CNC. a) Overview image. b) HRTEM image of a CNC tip over a hole in the holey carbon grid. c) Magnification of image in b) to show the groups of layers with separating cavities.

The images show a clear faceting of the layers at the tip of the CNC, with a broad tip. Cavities are visible in the structure, acting as independent tips separating uniform layers. Each group of layers are fairly uniform moving in from the edge towards the centre of the CNC, but at the cavity the apexes of each group of layers is different from the previous group.

Further in towards the first cavity from the tip, the layers seem to be more and more equal to the mathematically perfect cone wall, but still faceted to some degree, and with somewhat wide tip. Approaching each cavity where a wall is approaching a mathematically perfect SWCNC wall, the wall group stops.

The image show that there are cavities between each group of CNC walls with equal faceting and tip sharpness, but they do not seem to be occupied by any particle.

4.1.4 Unconfirmed Particles

During investigation of grinded and ion milled prepared sample 6, an interesting area was revealed and is shown in Figure 4.1–6.

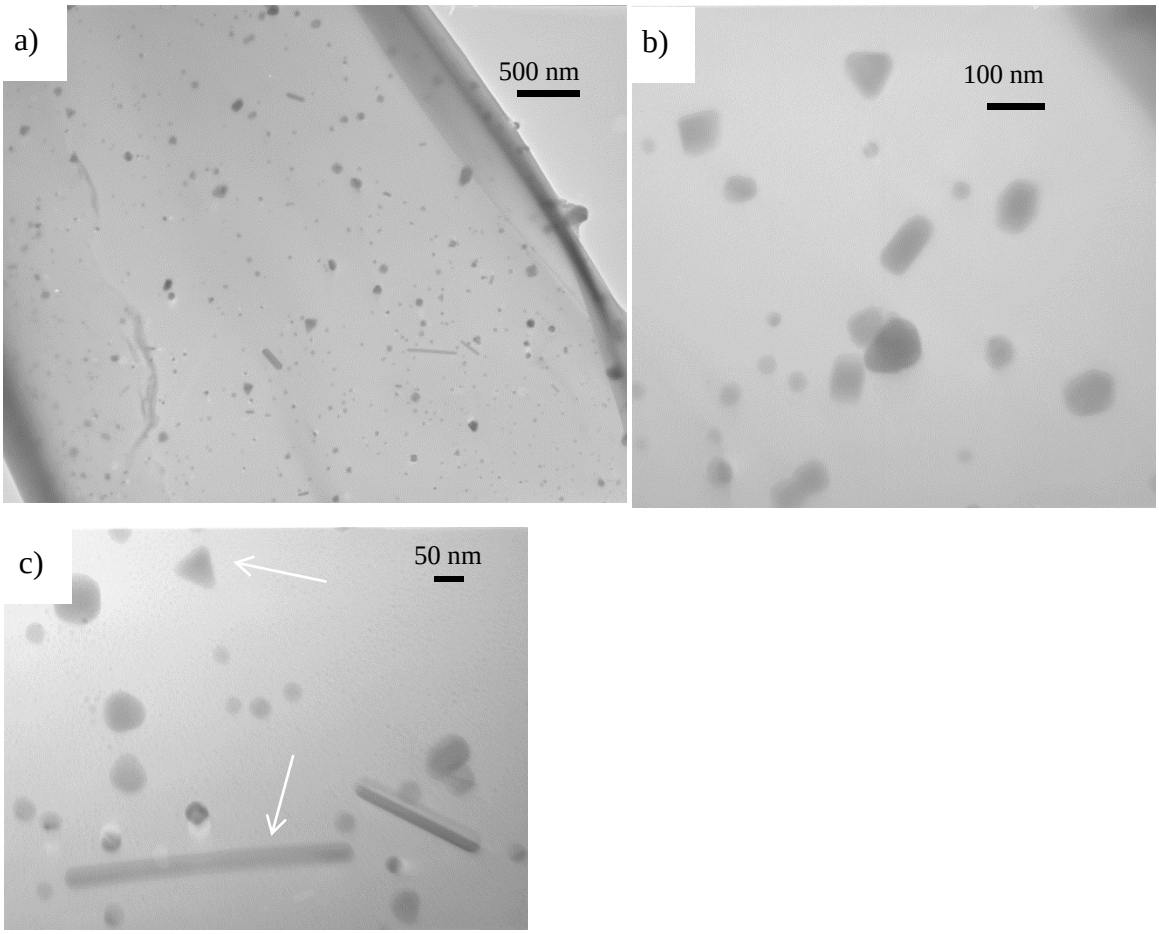

Figure 4.1–6: a) TEM overview image of a periphery part of an aligned sample. b) Larger magnification image showing possibly tilted small carbon nanocones. c) Larger magnification image of disks projected from the sides, and possibly small carbon nanocones which appear triangular in the image.

The triangular shapes on the picture, does not fit with any known size for carbon nanocones, with sides at roughly 60 nm. The shape of the particles does fit with a carbon

cone of an apex angle of 60° however. Several such triangular particles are seen in Figure 4.1–6 a).

No EDS was taken of the area, and the area was not located again at a later point to confirm the particles. Because of this, there is no conclusive evidence that these particles are actually carbon nanocones, and not contamination. As a counter argument, one could ask what contamination could generate particles which are projected as triangular shapes; or rather what is the probability of this.

If the particles can be interpreted as carbon nanocones, this would shed some light on a mystery about carbon nanocones. Researchers have earlier asked themselves why there have been no smaller carbon nanocones in the CB&H batch, if the particle formation is a seeding process. If the particles are grown gradually after seeding, particles should appear in a larger size distribution. It could be possible that the particles discovered are either in the batch and not discovered earlier because of methods and sample preparation, or the particles are inhomogeneously distributed in the batch, with a low concentration.

4.2 CNC and Polymer Wetting from Ethanol Dispersion

Figure 4.2–1 is a TEM image of sample 2, which show CNCs and polymer which were prepared by dispersion in ethanol.

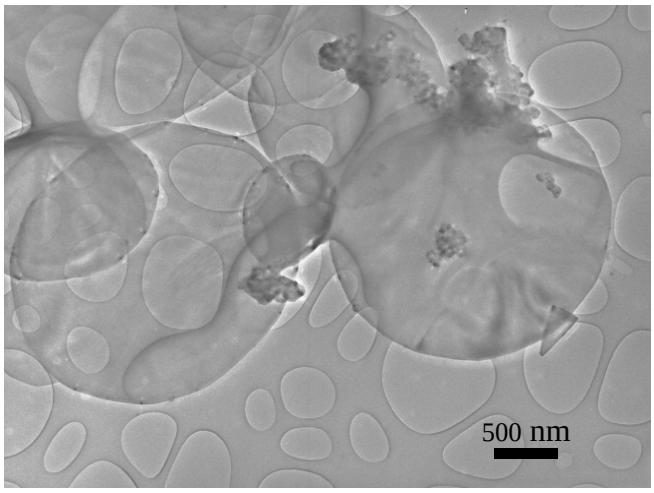

Figure 4.2–1: TEM image illustrating how the polymer interacts with the CNCs.

Interesting in the picture is how the polymer deposits as a layer onto the surface of the carbon, and not outside. It is obvious that the polymer has a distinct preference to the carbon. In addition, it is worth noting that the polymer connects the carbon, as long as there are particles which it can stick to.
This was the trend for all pictures on several samples made in the same way.

4.3 Preparation and Alignment of Polymer/Carbon Nanocones Composites

In order to investigate the inner structures of the polymer/CNCs composite, such composites was synthesized and aligned by dielectrophoresis as described in Section 3.1.

Figure 4.3–1 shows optical microscopy (OM) images of in-plane aligned sample C.

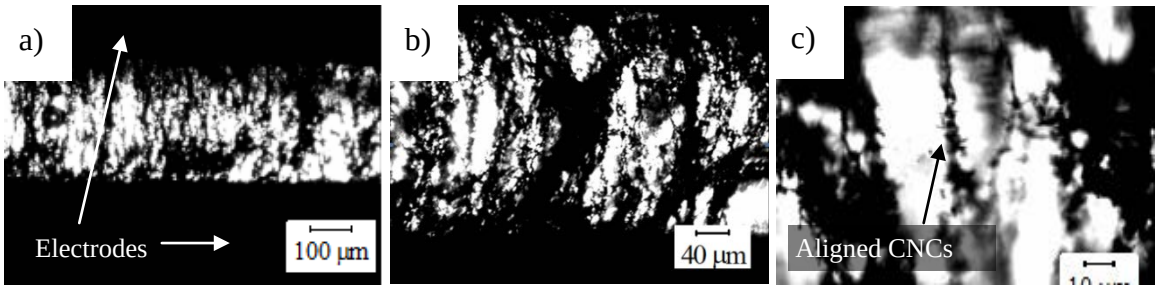

Figure 4.3–1: OM image of aligned particles between the two electrodes in-plane. The alignment direction is vertical in the image a) Overview image illustrating the general composite. b) Full lengths of the aligned wires shown. c) Close-up of a single wire of aligned particles.

While the images show that the composite is non-uniform and with wires of aggregated strings, the images show successful alignment and also some single chain stings. The non-uniformity most likely arises from the inhomogeneous field from either aggregates or faster growing chains, or it could be a result of mechanical instability issues like shaking which affected the growth.

Figure 4.3–2 shows the result of a similarly in-plane aligned composite but with another polymer, sample B. In the image one electrode has been removed. The polymer is amine-based like sample C, and alignment looks roughly equal.

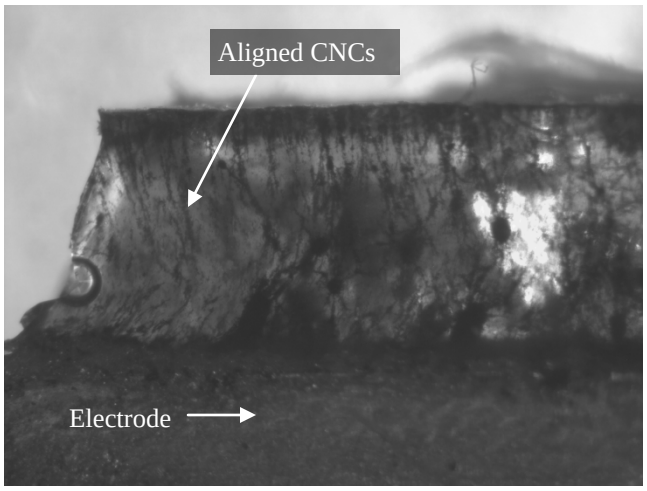

Figure 4.3–2: OM image of an in-plane aligned sample. One electrode has been removed, and at the left a piece of the composite has been removed.

In Figure 4.3–3, an out-of-plane aligned composite is shown to illustrate a typical setup before removal of electrodes.

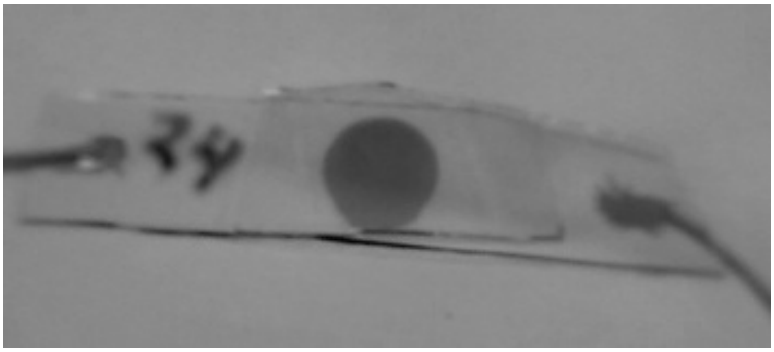

Figure 4.3–3: Image of out-of-plane aligned composite. The aligned composite is situated between the two ITO-coated glass pieces, as illustrated in Figure 3.1–1.

Out-of-plane composites are generally harder to achieve with the setup used than in-plane composites, due to the fact that there is no way to optically check for alignment. A quick conductivity check is hard to achieve without disturbing the alignment, sometimes a successful check may lead to low conductivity after curing because of this disturbance.

In-plane composites may also fail, either by disturbance or non-optimal setup parameters, or if the unhardened composite is displaced. Figure 4.3–4 shows such a badly aligned composite, with focus at the polymer which has spilled over the edge. This causes the carbon to move by DEP to the high field gradient at the silver polymer electrode contact shown at the bottom of the image. The new distribution caused by this disrupts the field-induced assembly in the area.

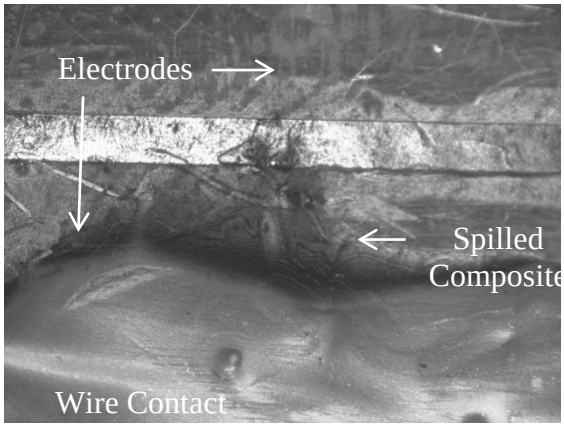

Figure 4.3–4: OM image of a failed sample. The polymer/carbon dispersion has spilled over the boundaries of the electrodes.

gation of the Composites

4.4.1 Grinding and Ion Milling

Figure 4.4–1 shows failed samples during ion-milling. Figure 4.4–1 a) show how a sample burst without a previous hole during ion-milling, sample.

Figure 4.4–1: OM images of failed samples. a) The edges towards the break indicate how the sample

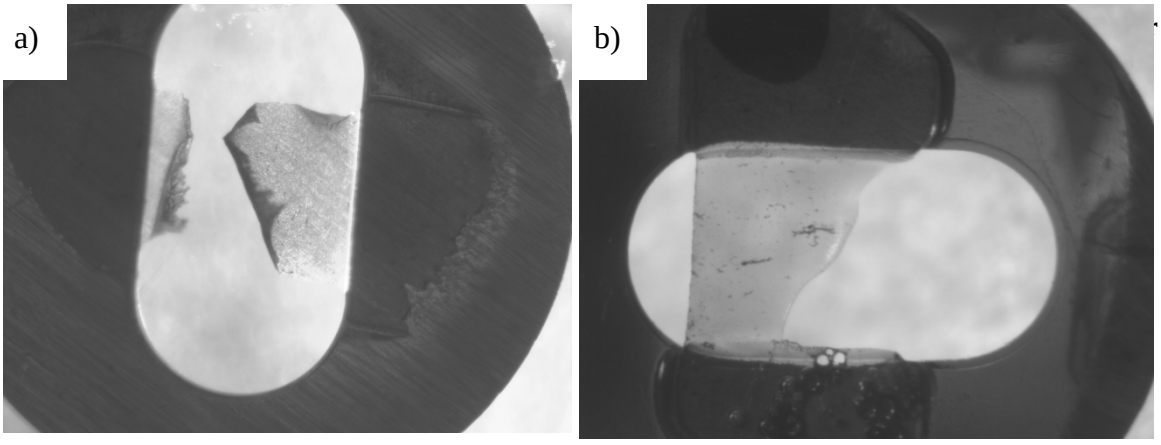

Since the edges of the broken area have distinctive edges in the middle, the burst must have started at the sides. The burst could have come from using badly aligned ion-guns/sample positioning which thinned the hole inhomogeneously so that the sides was thinner than the middle, but unlikely since the setup was aligned before use. The burst

can also have been caused by shrinkage of the polymer from the heating by bombarding with ions, or it could be an effect of structure strengthening chain fragments in some parts of the sample, causing it to simply break in the point of least resistance.
In Figure 4.4–1 a), carbon strengthening in the middle of the sample is indicated, since the edge is pointing out where the carbon concentration is higher.
The inhomogeneous strengthening causes the hole to be displaced; ruining the sample which TEM later showed was unusable because of too thick edges. The samples indicate that a thin sample with chain fragments would be difficult to achieve.

Further tries paid off, and Figure 4.4–2 shows a better sample. Although the hole is still misplaced, the sample was structurally rigid and with thin sloped edges.

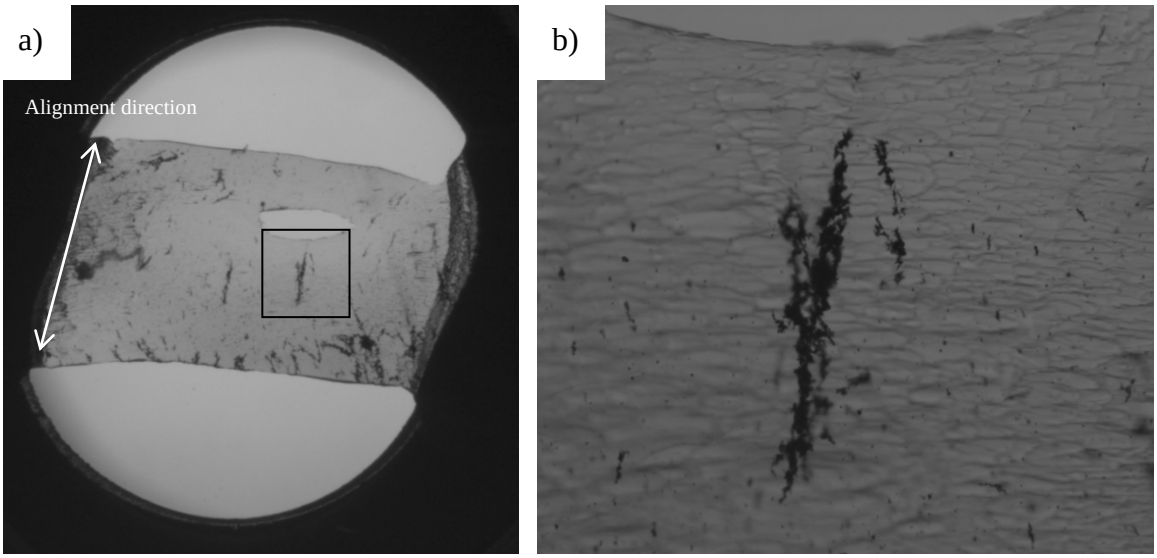

Figure 4.4–2: OM image of ion-etched sample. a) Overview image showing the position of the hole compared to the chain fragments. b) Chain fragments close to a hole, but too thick for TEM.

The sample did not reveal any good images of aligned CNCs, and Figure 4.4–2 b) show that the hole is misplaced compared to aggregated carbon chains.

Figure 4.4–3 shows images of the sample after further ion-milling.

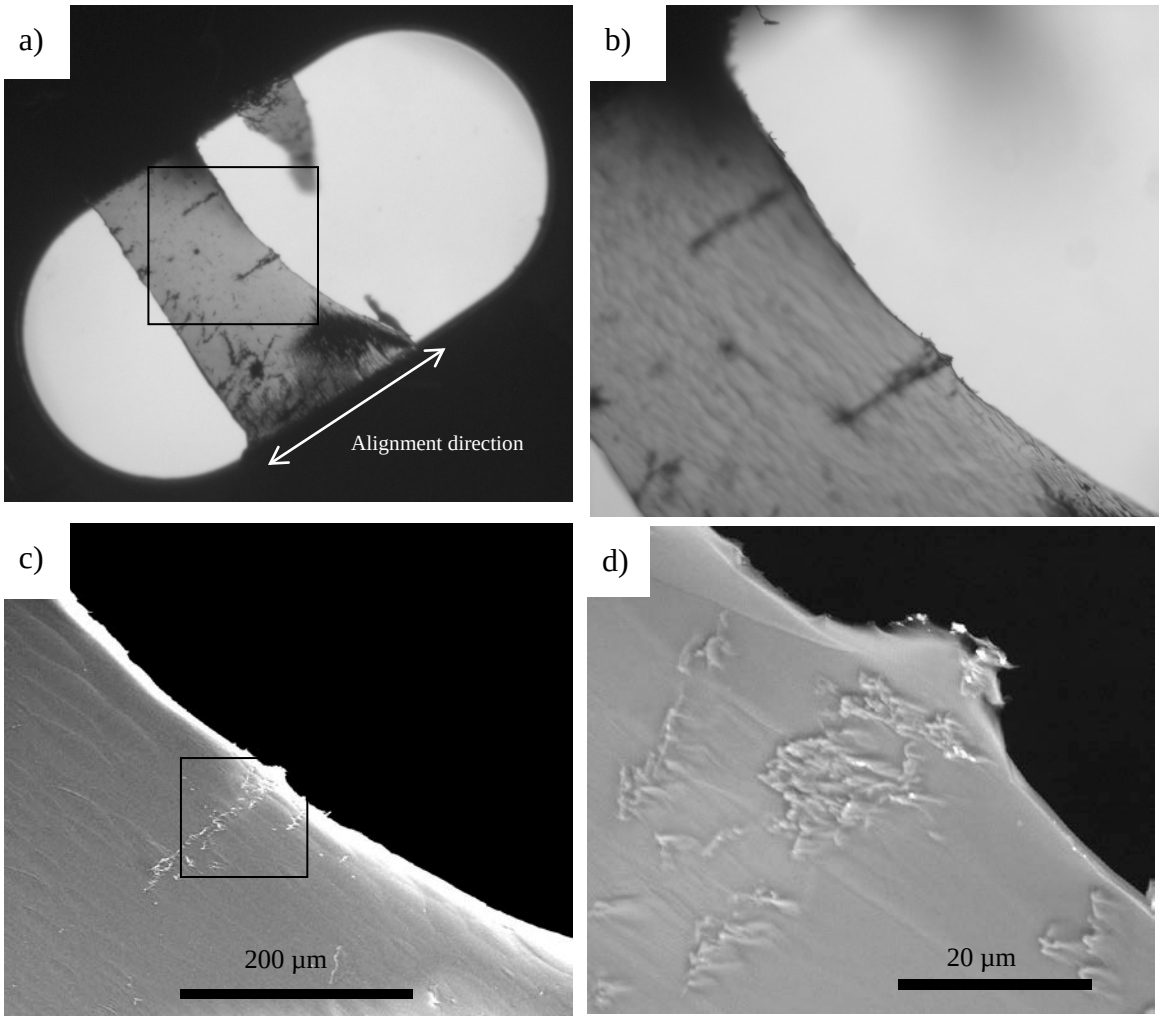

Figure 4.4–3: Aligned sample after ion-milling. a) OM image overview where chain fragments are clearly visible. b) Magnification of same sample showing how the chain fragment points out of the matrix. c) SE SEM image of the same area showing how the protrusions are above the chain fragments d) BSE SEM image showing the protrusions in higher magnification.

encapsulated in polymer. This also says something about the wetting properties of the polymer. If wetting was low or with physical defects, the polymer would have been gone from the particles which pointed out. In addition, SEM shows that protrusions are visible above the chain fragments on the surface, which is heavily bombarded with ions during milling. The chemical wetting, physical interface between polymer/CNC and general structure strengthening properties of the carbon must therefore be quite tough.

In Figure 4.4–4, TEM images from the tip of the previously presented sample are shown. The images show that at the very tip some CNCs are detectable, but the sample quickly becomes too thick for imaging.

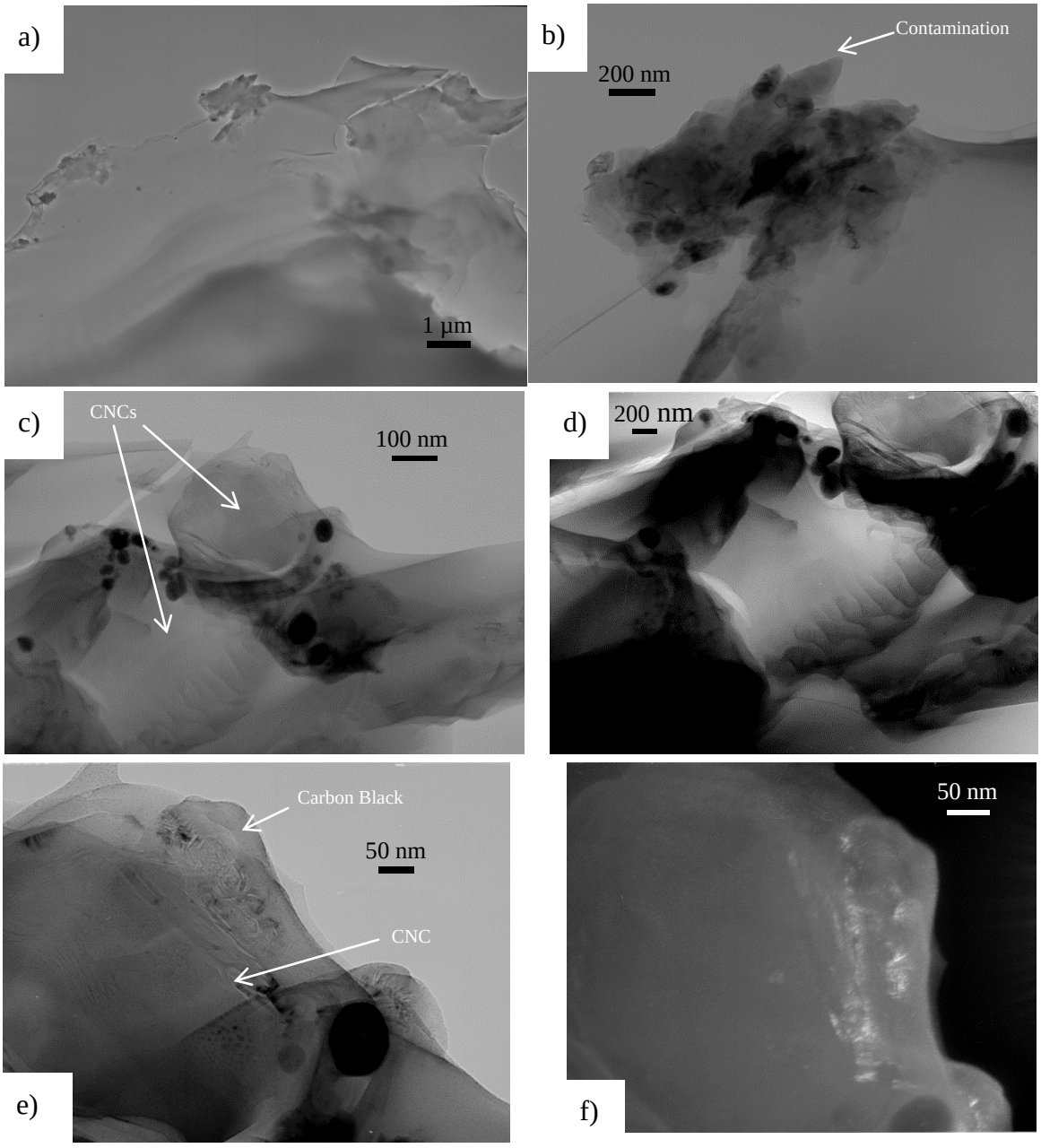

Figure 4.4–4: TEM images of ion-milled sample. a) Overview image of the tip of the chain covered with polymer. b) Contamination at tip. c) BF image of CNCs and CB particles. d) BF image of CNCs, with a polymer fringes at central CNC. e) BF image of a CNC and CB particles. f) DF image of a CNC and CB particles.

There are several other structures which may possibly be CNCs in the area, but contrast is too low with the thick sample. Semi-amorphous CB particles is also visible, and DF image in Figure 4.4–4 f) show the image formed by the reflection from these. From this, it can be confirmed that the particles in the vicinity are not of the same species.

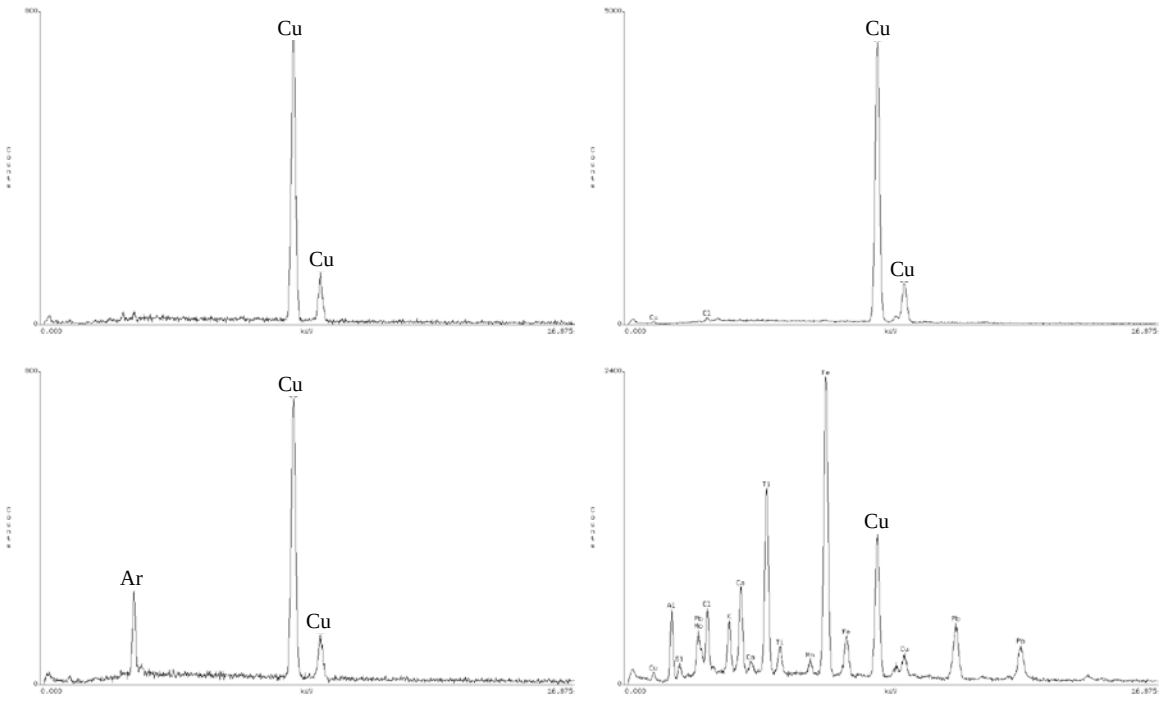

Figure 4.4–5: EDS results from ion-milled sample at: a) Thick area without CNCs. b) Round particles in polymer matrix. c) Area with a CNC. d) Contamination at the tip.

EDS from polymer and CNCs compared to the dark spots in the sample, confirms that the dark spots are copper rich, and likely to come from the copper ring during ion-milling.
In all the samples argon and copper peaks are visible, and is to expect from ion-milling where copper is at the copper ring, and argon is being bombarded onto the sample.
EDS from the area in Figure 4.4–4 d) however, show a broad spectre of elements and is most likely a contamination from the ion-milling sample holder or another external source from sample preparation.

The results from the methods show that for at least the specific sample it is difficult to sample prepare to view aggregated chains, since the aggregates are structure

strengthening towards ion-milling. It is possible that a decent sample can be prepared by the method for the specific purpose, but it is likely to be based on luck rather than predictability. There is still a possibility that single chains may be investigated by the method, as the chains have a smaller cross-section diameter.

4.4.2 Matrix-embedded Cross-sections

For matrix-embedded cross-sections, the embedding was successfully accomplished, but during ion milling, all samples were destroyed or rendered unsuitable for TEM. This occurred either by the embedding material loosening from the brass tube or the sample was milled off-centre due to inhomogeneities like air bubbles and structure-strengthening areas from CNCs in the composite.

4.4.3 Cryo- and Ambient-Ultramicrotomy

Cryo-Ultramicrotomy samples were successfully sectioned, although quite a lot of sections were unusable for TEM. Figure 4.4–6 shows SEM and TEM low magnification images of such sections. The images illustrate how the sections have curled and been destroyed, rendering it unusable, and also how there may be smaller areas which are usable for TEM.

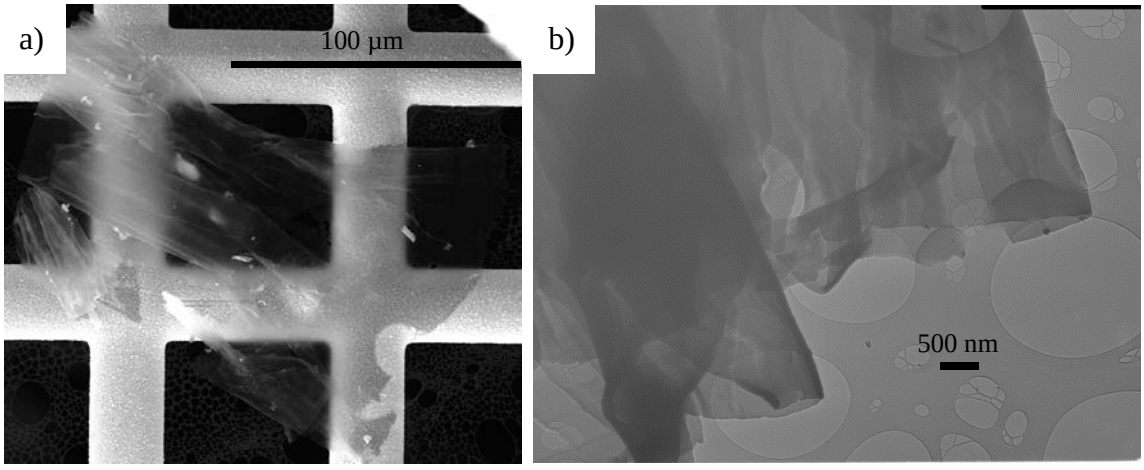

Figure 4.4–6: a) SEM image of a section from cryo-ultramicrotomy. Some usable areas are visible. b) TEM image of a curled section, illustrating an unusable sample.

Some sections gave good results in TEM, although with a generally low contrast. Figure 4.4–7 shows TEM images of aligned CNCs from sample 5.

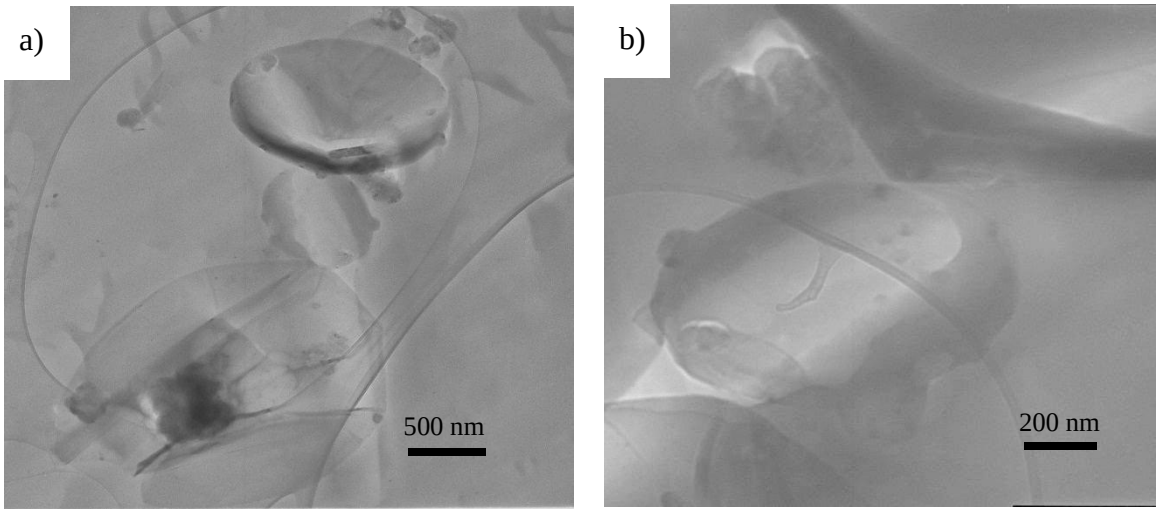

Figure 4.4–7: Aligned CNCs in a polymer matrix on a holey carbon grid. a) Overview image. b) Magnified and tilted sample to show the interface between particles.

The images show three disks and one cone aligned so that the particles are in an imaginary line, and with small CB particles dispersed along the surfaces. A small hole is also seen between two of the particles and possibly along the axis of alignment, seen as a brighter line. The centre disk seems to be in the possible polymer fracture.

By using the sample preparation method, similar samples also showed single particles spread in the sections, which is shown in Figure 4.4–8. These show examples of filling of polymers around the rim of the carbon nanodisks, with no visible gap between the particles and the polymer. Figure 4.4–8 shows two carbon nanodisks with approximate distance of 1.9 μm from edge to edge.

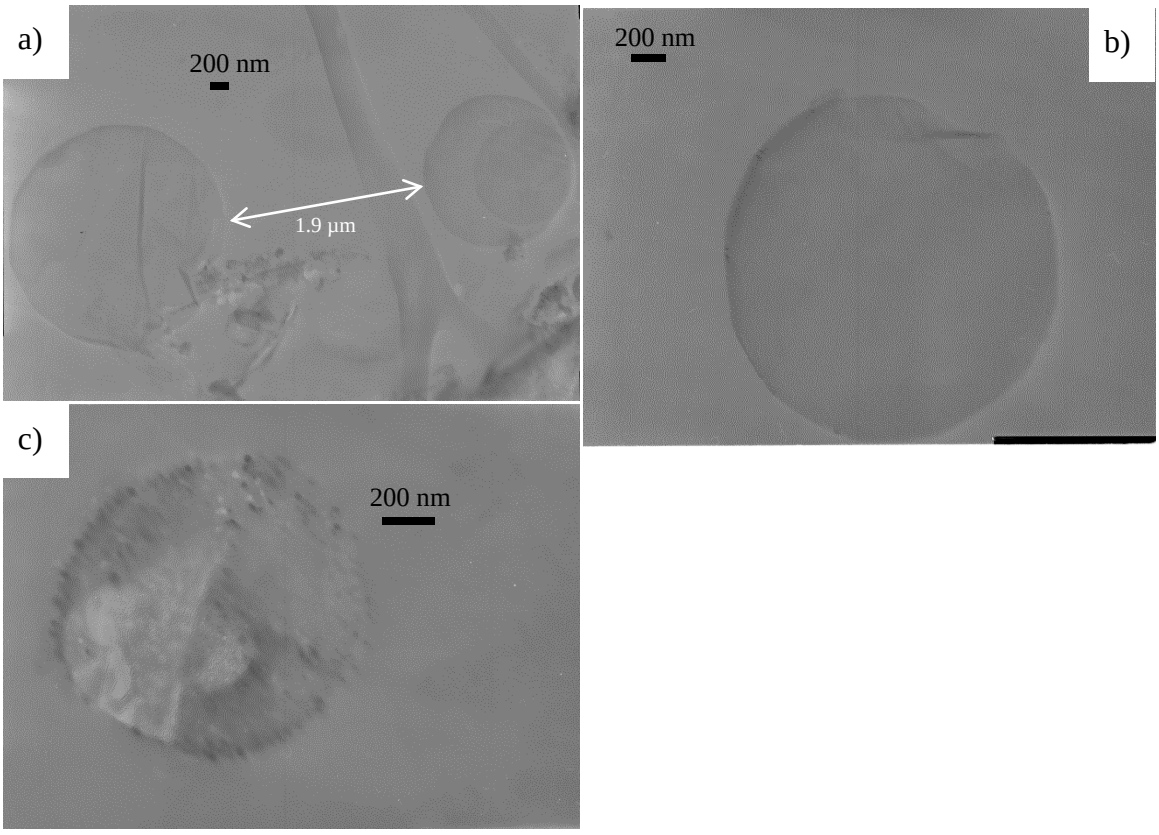

Figure 4.4–8: TEM images of carbon disks in polymer matrix. a) Three disks where two of them are stacked. b) A CNC showing no creeping along the circumference of the disk. c) CNC with CB particles attached, displaying uneven polymer thickness at the flat side.

4.4.4 Cross-sections

Figure 4.4–9 shows a failed cross-section made directly from the aligned sample with electrodes, sample 6.

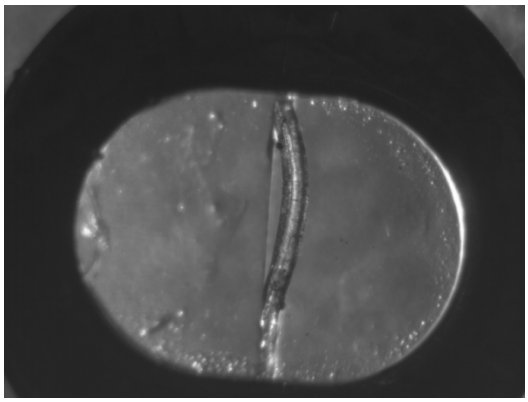

Figure 4.4–9: Optical microscopy image of failed cross-section.

The image show the general trend of the preparation method, where the composite did not maintain mechanical stability after grinding.

5. Discussion

5.1 The Structure of Carbon Nanocones

To simplify the descriptions and discussions about CNC structures, a nomenclature to distinguish the various facets of a CNC is proposed and shown in Figure 5.1–1.

The α-type facets are the principal structural facets along the cone wall of carbon nanocones from the apex to the circumference at the open-ended side of the cone, and along the circumference of a carbon nanodisk. β-Type facets are the nanostructural facets along the circumference of the carbon nanocones and disks.

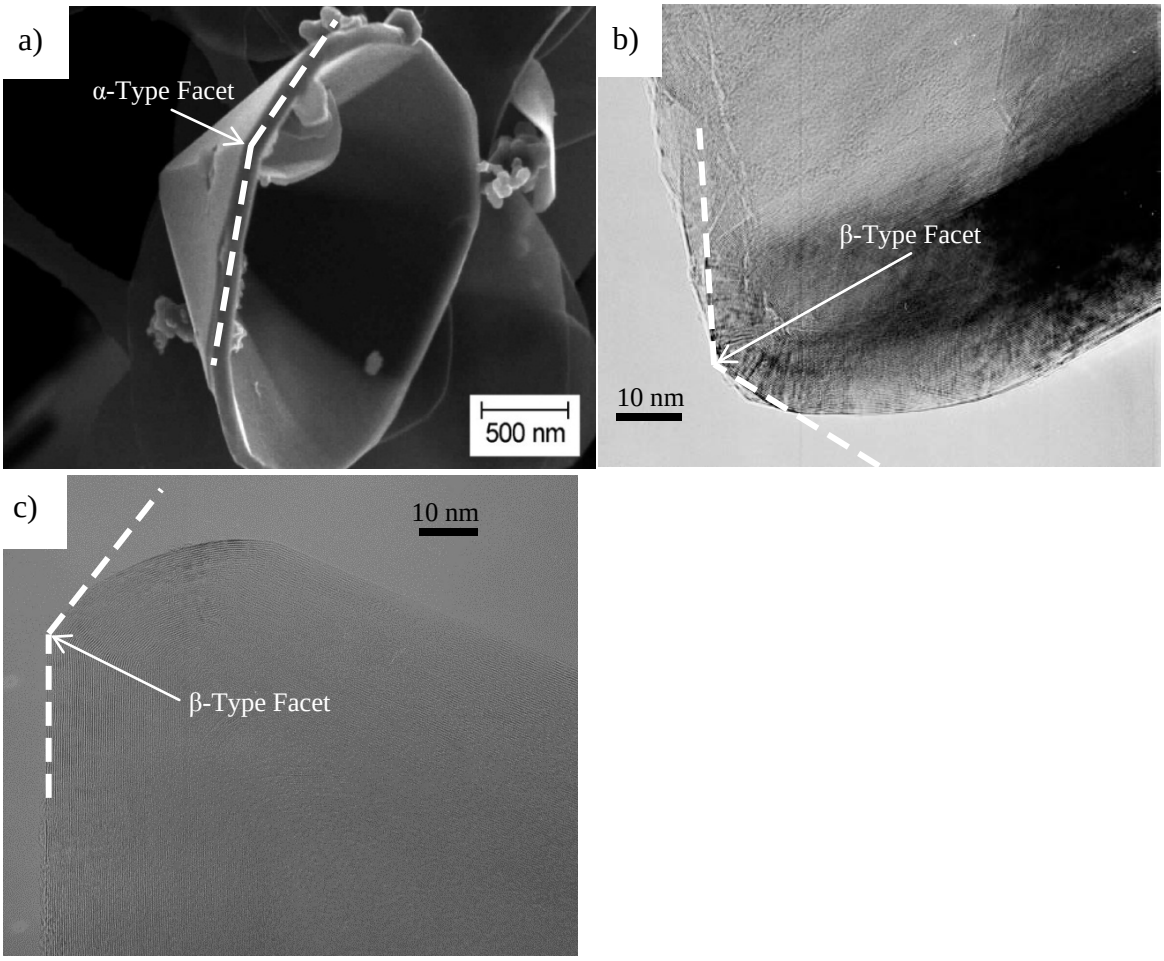

Figure 5.1–1: Various facets of a carbon nanocone. a) α-Type facet along the outer cone wall from the apex to the circumference of the open-ended side. b) β-Type facet along the circumference of the open-ended side. c) β-Type facet at the tip of a CNC. Picture in a) based on Knaapila *et al.* [2].

5.1.1 Circumferential Edge Structure

Figure 4.1–3 shows that the CNCs are not stacked SWCNCs, but the inner layers follow around the edge and are connected to the outer layers. This have previously been observed, but not reported [30].
These layers are shown as highly β-type faceted, and the images also show that the faceting is non-uniform around the circumference direction, seen by facets protruding from the predominant image layer.

If the facet planes are oriented in a direction so that the angle between the incident beam and the planes satisfies Bragg's law, diffraction contrast will be visible. Strong Bragg scattering at a specific location would cause dark areas at the facet position.
As the facet angles in Figure 4.1–3 are changing along the rim of the cone, this gives rise to local fulfilment. This is in agreement with the contrast seen in Figure 4.1–2 b), where the dark areas are distributed along the rim of the disk, with local fulfilment of Bragg's law.

The facets shown are very similar to the faceting at the tip of the CNCs, discussed further in section 5.1.3.
Most likely the CNCs were initially grown as mathematically perfect SWCNCs which grew further by deposition of carbon into BSUs. The β-type facets observed here are likely formed during the graphitization process where small BSU's are joined to form strict layers.

5.1.2 Layers

The wall structure of heat-treated CNCs has earlier been thoroughly investigated with HRTEM, and has shown that the structure is layered. As described in Section 2.1.2, previous results also have shown that the structure must be made initially of aligned and parallel BSUs of semi-amorphous carbon. The domains after graphitization have been reported previously to have coherence length of 20 nm within the graphite plane, and 17

nm perpendicular to the plane [13], but the measurements were performed by diffraction peak width calculations. Such results would vary greatly on the projection, and the interpretation.

FFT at various positions of a cone wall projected perpendicular to the layer direction, show that only the intensity of the spots varies while changing position along the surface, the position of the spots do not move. The direct interpretation of this is that none of the graphene sheets in the wall-structure has a variation perpendicular to the incident beam within the triangular area of investigation of about 300 nm^2. As there are about 100-150 graphene sheets in each wall structure [25], this indirectly means that the sheets do not have domain variations in the x,y-plane, and the sheets must therefore be continuous around the structure. The other solution is that none of the possible domains have a domain variation in that precise spot, which is very improbable with the amount of sheets.

5.1.3 Tip Structure

Section 4.1.3 show a HRTEM image of a regular CNC with a discrete apex angle, and from theory one would assume this means all layers are stacked cones of graphene sheets with apex angle arising from the number of pentagons at tip.
The image however, shows that most of the layers are not like this at all. There may be some layers in some CNCs which fit the previously mentioned model, but most of the layers have a different morphology. The outer layers are highly β-type faceted, meaning that the tip is not round edged but instead it has several distinct corners. These layers must have symmetry of several pentagons in a complex pattern to enable this, but as the image show; it is not random tip geometry either, since there is a wide area of similar layers going towards the core.

As mentioned, no layer in the cone is the structure of a mathematically perfect SWCNC. Most likely, there is such a SWCNC in the centre of the CNCs in the start of the growth process; otherwise the particles would not take forms with such distinct apex angles.

These SWCNCs have probably later grown by deposition of small BSUs or close to amorphous carbon around the core. Recrystallization of the particle either during growth or graphitization has likely changed the structure to the one observed here. This is interesting compared to the β-type facets in section 5.1.1, as the facets are very similar, and probably of the same origin.

There have been suggestions earlier that the seeding of CNCs arise from particles so that the CNCs build around these, comparable to how CNTs grow. The HRTEM image shows no particle neither in the centre of the CNC, nor in the cavities.
This challenges of the theory that the CNC may be seeded by a particle.

5.2 Polymer/CNC Surface Interface

Cryo-Ultramicrotomy results in Figure 4.4–8 shows that there is no visible open space between the carbon nanodisks and the polymer, neither along the circumference, nor on the flat side. With regards to the carbon nanocones, images show that there are no visible open space between the polymer and the outer side of the cone. Images does not show clearly any sign if this is the same case on the inside of the cone, i.e. if the polymer fills the inside of the cone or not.

Investigation of polymer and CNCs dispersed in ethanol by TEM proved to be a good method for discovering some properties of the interaction. Although the contact angles between polymer and the carbon surfaces were not measured, the method proved sufficient for the purpose. The investigation shows that the polymer have tendency to form as a layer on top of the CNCs instead of generating polymer agglomerates, at least at the concentrations used.

The ethanol dispersion experiment has impact on the question if the filling in the interface of single particles from ultra-microtomy is predominantly caused by electrowetting [40] during dielectrophoresis or not. As the ethanol dispersion showed a

similar interface without any applied electrical field, this concludes that electrowetting is not the predominant factor.

5.3 TEM Sample Preparation Methods for Aligned ACAs

To find a good TEM sample preparation method, several methods and techniques were used. This section discusses the results shown section 4.4 and the way to develop a method for sample-preparation of the composite.

5.3.1 Ultramicrotomy

Preliminary tests of UM sectioning showed that the CNCs in the composite ripped the sections. The reason for this is that the polymer is quite soft compared to the rigid and hard CNCs. These therefore act at the sectioned sample like an imperfect diamond knife would at the points where the knife hit a particle, instead of cutting through the particles. As UM sections were cut to about 70 nm while CNCs are in the range of about 200 nm – 4000 nm, this means most particles are displaced by the knife except the ones in-plane with the section. As investigation of a chain of aligned CNCs require a minimum of two particles close to each other not to be displaced, this is statistically very unlikely to generate such results. The results conclude that the method is not viable for polymer/ carbon nanocone alignment investigation.

5.3.2 Cryo-Ultramicrotomy

As Ultramicrotomy results concluded that it was an unviable method for the purpose, cryo-UM was chosen as the next method. Since the problem with Ultramicrotomy was that the particles were too hard compared to the polymer and causing destruction of the sections, a route to eliminate the problem was chosen. Cryo-Ultramicrotomy utilize low temperature cutting, and these temperatures would make the polymer harder during the cutting process.

Cryo-UM without a collection bay is a mechanically harsh process since the slices are curled up on the blade, so most sections were destroyed by tearing on macro-scale or folded such that the sample was too thick. A couple of sections were successful however, and showed that the method was seemingly working, as those sections had a small area of flat single-layered section. TEM imaging in those areas showed various CNCs in the polymer matrix with no or very little tearing on a micro-scale from CNCs being displaced.

Figure 4.4–8 shows single particles in a polymer matrix. Although the images show that the particles are not in contact they could still be a part of the same carbon chain. The carbon chains in the composite are not perfectly one-dimensional, but the quasi one-dimensional chain may have any direction at a single point in the matrix. Since the sample preparation method is only two-dimensional, the particles described may be still of the same chain. The distance between the particles in Figure 4.4–8 a) is approximately the same as the diameter of a CNC, which indicates the theory is correct in this instance.

Figure 4.4–7 show CNCs aligned in the polymer matrix, where three disks and one cone constitute the part of the chain. The particles have a point contact rather than a larger flat surface contact area. In the prepared sample, the contacts seemed to occur at the singular points of the particles, that is the facets of disk edges and cones, and at the apex for the carbon cones. The result may explain why the conductivity of the composite is so fragile, as mechanical stress easily disrupts point contact of the particles.

Carbon black particles also seem to be a part of the alignment as theory predicts, and in Figure 4.4–7 they seem to be more abundant in the space between the CNCs than other places. Whatever this is a coincidence or not is hard to tell, but it can be justified by theory, as the bigger particles create a local field from polarization, the alignment direction have a larger field gradient then other directions. Such gradients could just as well cause propagation of smaller particles like carbon black between aligned larger particles. As the particles are quite small, it is possible that the movement

There is a chance that two CNCs close to each other might be a statistical event of randomly positioned CNCs. As for four CNCs in the close proximity shown here, the probability that the particles that close positioned and oriented is very low.

5.3.3 Grinding and Ion Milling

Initial methods for sample preparation included grinding of in-plane aligned composites.
Like for ultramicrotomy, mechanical grinding also suffered from particles being very hard compared to the polymer matrix, causing displacement and tearing at the surface. Grinding was also complicated by interaction with acetone which was a part of the grinding technique. Composite prepared with polymer AY105-1 proved to interact with acetone when it was grinded sufficiently thin. After a lot of tweaks in the preparation method, the polymer was switched. Composites prepared with polymer G1 were proven stable, and after extensive amounts of attempts of preparation TEM images were produced by grinding and ion milling.
These images showed that the chain of CNCs were structure-strengthening with regards to ion-milling, which also SEM images showed later on. While some areas were able to be milled down to a thin enough sheet, the areas with the CNC chain were too thick for internal imaging. Close to the tip of the chain tough, there were several CNCs close to each other confirmed by diffraction, as well as CB particles.
Outside of the tip area, impurities were discovered by EDS, most likely from contamination during ion milling. Argon and Copper were discovered in the entire sample, which is likely from ion milling, copper from the copper ring.

After TEM investigation, it was discovered that the samples could successfully be re-ion milled, to move the position of the TEM thin area as one would expect for other samples.

5.3.4 Matrix-embedded Cross-sections

To maximize control of the TEM sample, matrix embedding was used. The idea was based on a previous publication [41] on similar problems with oriented materials.

Embedding the composite in a matrix was successfully done, but during ion milling the embedding was too unstable. Over a long series of attempts the adhesion between brass tube and matrix polymer was poor, the matrix polymer shrunk or the adhesion between composite and matrix polymer was poor. The milling point of the ion etcher was unforeseeable due to variations/interfaces from mass or air bubbles, both air in matrix polymer from embedding and structure-strengthening areas from CNCs in composite. In total these hindrances all contributed to making the sample preparation too unstable or unpredictable to continue.

5.3.5 Cross-sections

A common problem with aligned ACAs is that after the electrodes have been removed, the contact between the adhesive and another surface is often very much worse. Most likely, the conduction loss is due to either contact loss between an end-of-chain CNC and the electrode, or mechanical stress in the polymer close to the electrode when separated causing local loss of conductivity. To understand the mechanics of this, it would be interesting to investigate the interface between the electrodes and the composite without removing the electrodes.

To achieve this, a simple method of cross-sectioning was chosen by using the adhesive used in the alignment as the only adhesion to the glass. The result was in all cases, that the adhesion between the glass and the polymer was too low to withstand the mechanical stress of grinding, as the image in Figure 4.4–9 shows. The problem may also have been caused by acetone softening the polymer from the mount-grinding technique, although the polymer should be stable in this environment. Substantial amount of time was used to attempt to make a cross-section which did not have the flaw, but the method proved unsuccessful for the purpose.

6. Conclusion

In-plane and out-of-plane conductive polymer/carbon nanocone adhesives were successfully prepared by dielectrophoretic alignment of particles induced by an external AC source. Selected sample preparation routes for TEM were tested to establish a working method of investigation to discover the inner structure of the composites. By the routes and setup shown in the thesis several proved unsuccessful and unsuitable for the purpose, mostly because of structure-strengthening properties of the aligned carbon in the polymer during ion milling. Cryo-ultramicrotomy proved to be a successful method, although at a mediocre success rate and with limited area for investigation.

Cryo-ultramicrotomy prepared samples were investigated by TEM, and revealed that the particles have a point contact rather than a larger flat surface contact. In the prepared sample, the contacts seem to occur at the singular points of the particles, that is facets of disk edges and cones, and at the apex for the carbon cones. The point contact of the particles may explain why the electrical conductivity of aligned composites is easily disrupted by mechanical stress.

The wetting and filling of polymer/carbon were investigated by TEM, which qualitatively showed good wetting of polymer on the surface. The filling of polymer around the carbon nanocones and disks showed no cavities or polymer shrinkage at the interface between the particles and the polymer.

CNCs were also investigated by HRTEM, and several interesting results were discovered. The tip of the CNCs was shown to have facets, with subsequent layers having the same layer faceting and adding up to a group of layers. Such groups of layers were shown to be divided by cavities in the tip which separates the groups with different faceting.
Facets at the circumference of the CNCs were discovered, and these β-facets were also shown to be highly non-uniform along the circumference of the CNCs. The layered structure of CNCs was discovered to have no domain-changes within a relatively large area, indicating single-domain layers throughout the particle.

7. The Way Onwards

There are a lot of different questions which have not been answered in the specific field of science, both with regards to CNCs themselves and the polymer/CNC aligned composites.
To investigate polymer/CNC aligned composites further, Focused Ion Beam (FIB) technique would be very interesting tool to prepare a highly specific and controlled sample preparation method for TEM. Results in this thesis have shown that ion milling can reveal CNC aligned chain fragments for SEM, which could aid to make FIB possible without any staining.
The mechanical properties of the composites themselves on the nano- or micro-scale would also be quite interesting, to see if the structure strengthening abilities with regards to ion-milling also extends to increased mechanical properties.

To continue the work with regards to composite/electrode interface, the next step forward could be to investigate the material by cross-section of an out-of-plane aligned composite by using the same method as described in section 3.2.6 while using a more stable polymer like the polymer used in section 3.2.4. This method could any distribution or aggregation of wires at the electrode interface, and also the contact interface between the electrodes and the carbon strings.

An interesting next step of investigating CNCs further would be to calculate the curvature of the cones and compare to theory. This could possibly be accomplished in TEM by FFT along a line from the apex to the open-ended base, and calculating the eccentricity of the elliptical patterns.

On the nanoscale the CNCs would also be very interesting for investigation by a nano manipulator for SEM to reveal the real conductivity for the various CNC structures singularly, and by measuring particle interface resistivity in embedding exposing the particles by chemical etching or partial pyrolysis.

8. References

[1] Heiberg-Andersen, H., S, W. G., Skjeltorp, A. T. Graphene Cones. In: *Handbook of Nanophysics: Functional Nanomaterials*. Boca Raton: Taylor & Francis, 2011.

[2] Knaapila, M., Romoen, O. T., Svasand, E., Pinheiro, J. P., Martinsen, O. G., Buchanan, M., Skjeltorp, A. T., Helgesen, G. *Conductivity enhancement in carbon nanocone adhesive by electric field induced formation of aligned assemblies*. ACS Appl. Mater. Interfaces. 2011;**3**(2):378-384.

[3] Li, Y., Moon, K.-s., Wong, C. P. Nano-conductive Adhesives for Nano-electronics Interconnection. In: *Nano-Bio- Electronic, Photonic and MEMS Packaging*. New York: Springer Science+Business Media, LLC, 2010, p. 19-45.

[4] Li, Y., Wong, C. P. *Recent advances of conductive adhesives as a lead-free alternative in electronic packaging: Materials, processing, reliability and applications*. Materials Science and Engineering: R: Reports. 2006;**51**(1–3):1-35.

[5] Lyons, A. M., Dahringer, D. W. Electrically Conductive Adhesives. Second ed. New York: Taylor & Francis, 2003.

[6] Høyer, H., Knaapila, M., Kjelstrup-Hansen, J., Liu, X., Helgesen, G. *Individual strings of conducting carbon cones and discs in a polymer matrix: Electric field-induced alignment and their use as a strain sensor*. J. Polym. Sci., Part B: Polym. Phys. 2011;**50**(7):477.

[7] Moon, S., Sigmarsson, H. H., Huang, Y., Bruemmer, T., Khanna, K., Chappell, W. J. *Magnetically aligned anisotropic conductive adhesive for microwave applications*. IEEE Trans. Microwave Theory Tech. 2008;**56**(12):2942-2949.

[8] Knaapila, M., Hoyer, H., Svasand, E., Buchanan, M., Skjeltorp, A. T., Helgesen, G. *Aligned carbon cones in free-standing UV-Curable polymer composite*. J. Polym. Sci., Part B: Polym. Phys. 2011;**49**(6):399-403.

[9] Lewis, H. J., Coughlan, F. M. *An overview of the use of electrically coonductive adhesives as a solder replacement*. Journal of Adhesion Science and Technology. 2008;**22**:801-813.

[10] Iijima, S., Yudasaka, M., Yamada, R., Bandow, S., Suenaga, K., Kokai, F., Takahashi, K. *Nano-aggregates of single-walled graphitic carbon nano-horns*. Chem. Phys. Lett. 1999;**309**(3-4):165-170.

[11] Gogotsi, Y., Gogotsi. *Conical crystals of graphite*. Carbon. 2002;**40**(12):2263-2267.

[12] Jaszcak, J. A., Robinson, G. W., Dimovski, S., Gogotsi, Y. *Naturally occurring graphite cones*. Carbon. 2003;**41**(11):2085-2092.

[13] Naess, S. N., Elgsaeter, A., Helgesen, G., Knudsen, K. D. *Carbon nanocones: wall structure and morphology*. Sci. Technol. Adv. Mater. 2009;**10**(6):065002.

[14] Barth, W. E., Lawton, R. G. *Dibenzo[ghi,mno]fluoranthene*. J. Am. Chem. Soc. 1966;**88**(2):380.

[15] Balaban, A. T., Klein, D. J., Liu, X. *Graphitic cones*. Carbon. 1994;**32**(2):357-359.

[16] Ge, M., Sattler, K. *Observation of fullerene cones*. Chem. Phys. Lett. 1994;**220**(3-5):192-196.

[17] Krishnan, A., Dujardin, E., Treacy, M. M. J., Hugdahl, J., Lynum, S., Ebbesen, T. W. *Graphitic cones and the nucleation of curved carbon surfaces*. Nature. 1997;**388**:451-454.

[18] Bakken, J. A., Jensen, R., Monsen, B., Raaness, O., Wærnes, A. N. *Thermal plasma process development in Norway*. Pure & Appl. Chem. 1998;**70**(6):1223-1228.

[19] Smith, P. A., Nordquist, C. D., Jackson, T. N., Mayer, T. S. *Electric-field assisted assembly and alignment of metallic nanowires*. Applied Physics Letters. 2000;**77**(9):1399.

[20] Prasse, T., Flandin, L., Schulte, K., Bauhofer, W. *In situ observation of electric field-induced agglomeration of carbon black in epoxy resin*. Applied Physics Letters. 1998;**72**(22):2903.

[21] Sharma, A., Bakis, C. E., Wang, K. W. *A new method of chaining carbon nanofibers in epoxy*. Nanotechnology. 2008;**19**(32):325606.

[22] Chen, X. Q., Saito, T., Yamada, H., Matsushige, K. *Aligning single-wall carbon nanotubes with an alternating-current electric field*. Applied Physics Letters. 2001;**78**(23):3714-3716.

[23] Svåsand, E., Helgesen, G., Skjeltorp, A. T. *Chain formation in a complex fluid containing carbon cones and disks in silicone oil*. Colloids Surf., A. 2007;**308**(1):67-70.

[24] Park, C., Wilkinson, J., Banda, S., Ounaies, Z., Wise, K. E., Sauti, G., Lillehei, P. T., Harrison, J. S. *Aligned single-wall carbon nanotube polymer composites using an electric field*. J. Polym. Sci., Part B: Polym. Phys. 2006;**44**(12):1751.

[25] Garberg, T., Naess, S. N., Helgesen, G., Knudsen, K. D., Kopstad, G., Elgsaeter, A. *A transmission electron microscope and electron diffraction study of carbon nanodisks*. Carbon. 2008;**46**(12):1535-1543.

[26] Oberlin, A. *Carbonization and graphitization*. Carbon. 1984;**22**(6):521.

[27] Harris, P. J. F. *New Perspectives on the Structure of Graphitic Carbons*. Critical reviews in solid state and materials sciences. 2005;**30**(4):235-253.

[28] Klein, D. J., Balaban, A. T. *The Eight Classes of Positive-Curvature Graphitic Nanocones*. J. Chem. Inf. Model. 2006;**46**(1):307-320.

[29] Terrones, H. *Curved graphite and its mathematical transformations*. J. Math. Chem. 1994;**15**:143-156.

[30] Haage, F. *Unpublished results*.

[31] Yim, M. J., Li, Y., Moon, K.-s., Paik, K. W., Wong, C. P. *Review of recent advances in electrically conductive adhesive materials and technologies in electronic packaging*. J. Adhes. Sci. Technol. 2008;**22**(14):1593-1630.

[32] Pohl, H. A. *The motion and precipitation of suspensoids in divergent electric fields*. J. Appl. Phys. 1951;**22**(7):869-871.

[33] Bruus, H. *Theoretical microfluidics*. Oxford: Oxford University Press, 2008.

[34] Dimaki, M., Bøggild, P. *Frequency dependence of the structure and electrical behaviour of carbon nanotube networks assembled by dielectrophoresis*. Nanotechnology. 2005;**16**(6):759-763.

[35] Schwarz, M.-K., Bauhofer, W., Schulte, K. *Alternating electric field induced agglomeration of carbon black filled resins*. Polymer. 2002;**43**(10):3079-3082.

[36] Olsen, A. *The Theory and Practice of Analytical Electron Microscopy in Materials Science*. Oslo: Department of Physics, University of Oslo, Norway, 2008.

[37] Williams, D. B., Carter, C. B. *Transmission electron microscopy: A textbook for materials science*. New York: Springer, 2009.

[38] Michler, G. H. *Electron Microscopy of Polymers*. Berlin, Heidelberg: Springer-Verlag, 2008.

[39] Roos, N., *Acknowledged for cutting sections at the electron microscopy unit for Biological sciences, University of Oslo.*

[40] Jones, T. B. *On the Relationship of Dielectrophoresis and Electrowetting*. Langmuir. 2002;**18**:4437-4443.

[41] Müller, E., Krumeich, F. *A simple and fast TEM preparation method utilizing the pre-orientation in plate-like, needle-shaped, and tubular materials*. Ultramicroscopy. 2000;**84**(3-4):143-147.